Molecular Therapy
Oncolytics
Original Article

Acquired chemoresistance can lead to increased resistance of pancreatic cancer cells to oncolytic vesicular stomatitis virus

Dakota W. Goad,[1] Christian Bressy,[1] Molly C. Holbrook,[1] and Valery Z. Grdzelishvili[1,2]

[1]Department of Biological Sciences, University of North Carolina at Charlotte, 9201 University City Blvd, Charlotte, NC 28223, USA; [2]School of Data Science, University of North Carolina at Charlotte, Charlotte, NC 28223, USA

Vesicular stomatitis virus (VSV) is a promising oncolytic virus (OV) against different malignancies, including pancreatic ductal adenocarcinoma (PDAC). Our previous studies have demonstrated that VSV-based OVs are effective against the majority of tested human PDAC cell lines. However, some PDAC cell lines are resistant to VSV. PDAC is one of the deadliest types of human malignancies in part due to intrinsic or acquired chemoresistance. Here, we investigated how acquired chemoresistance impacts the efficacy of VSV-based OV therapy. Using an experimental evolution approach, we generated PDAC cell lines with increased resistance to gemcitabine and examined their responsiveness to oncolytic virotherapy. We found that gemcitabine-resistant PDAC cells become more resistant to VSV. The cross-resistance correlated with upregulated levels of a subset of interferon-stimulated genes, resembling the interferon-related DNA damage resistance signature (IRDS), often associated with resistance of cancer cells to chemotherapy and/or radiation therapy. Analysis of ten different PDAC cell lines showed that four PDAC cell lines most resistant to VSV were also highly resistant to gemcitabine, and they all displayed IRDS-like expression in our previous reports. Our study highlights a possible interaction between two different therapies that should be considered in the future for the development of rational treatment regimens.

INTRODUCTION

Oncolytic virus (OV) therapy is an emerging anticancer approach that utilizes replication-competent viruses to preferentially infect, replicate in, and kill cancer cells. There are currently three OVs approved for clinical use: talimogene laherparvec (T-Vec) (based on herpes simplex virus 1) approved in the United States and European Union for melanoma,[1] Rigvir (based on enteric cytopathic human orphan virus 7) approved in Latvia and several other countries for melanoma,[2] and Gendicine (based on adenovirus type 5) approved in China for head and neck squamous cell carcinoma.[3]

Vesicular stomatitis virus (VSV) is a nonsegmented negative-strand (NNS) RNA virus (order *Mononegavirales*, family *Rhabdoviridae*, genus *Vesiculovirus*) and is a promising OV that is already in stage I clinical trials against various malignancies (Clincaltrials.gov trials NCT01628640, NCT03865212, NCT03120624, NCT02923466, NCT03647163, and NCT03017820). VSV is able to infect and replicate in a large variety of cell types.[4] The pantropism exhibited by VSV is largely due to its use of ubiquitously expressed cell surface molecules for attachment and entry to host cells, such as low-density lipoprotein receptor,[5] phosphatidylserine,[6,7] sialoglycolipids,[8] and heparan sulfate.[9] The oncoselectivity of most OVs, including VSV, is mainly due to defective or suppressed type I interferon (IFN) mediated antiviral responses in many cancers,[10–12] because most type I IFN responses are antiproliferative, antiangiogenic, and proapoptotic.[13]

This study focuses on pancreatic ductal adenocarcinoma (PDAC), which is one of the deadliest forms of cancer and is the number four cause of cancer-related death in the U.S. since the 1970s. The 5-year survival rate for PDAC patients is about 10%, whereas many other cancer types have significantly improved.[14] The poor survival rate for PDAC is largely attributed to late diagnoses and limited treatment options, as most PDAC tumors are either intrinsically resistant to chemotherapy or rapidly acquire resistance.[15] The mechanisms of chemoresistance are not fully understood and are likely multifactorial.[16]

Our previous studies showed that VSV is effective against most human PDAC cell lines, both *in vitro* and *in vivo*.[17] However, we also reported that some PDAC cell lines are resistant to VSV-mediated infection, replication, and/or oncolysis due to multiple mechanisms, including an upregulated expression of type I IFNs and/or interferon-stimulated genes (ISGs),[18–20] reduced viral attachment,[21] and/or resistance to virus-mediated apoptosis.[22] Our laboratory also demonstrated multiple strategies to overcome these mechanisms of resistance to OV therapy.[21,23]

Chemoresistant PDAC is a major hurdle and a key reason for the poor survival outcomes of PDAC patients. One important question

Received 29 September 2021; accepted 27 November 2021;
https://doi.org/10.1016/j.omto.2021.11.019.

Correspondence: Valery Z. Grdzelishvili, Department of Biological Sciences, University of North Carolina at Charlotte, 9201 University City Blvd, Charlotte, NC 28223, USA.
E-mail: vzgrdzel@uncc.edu

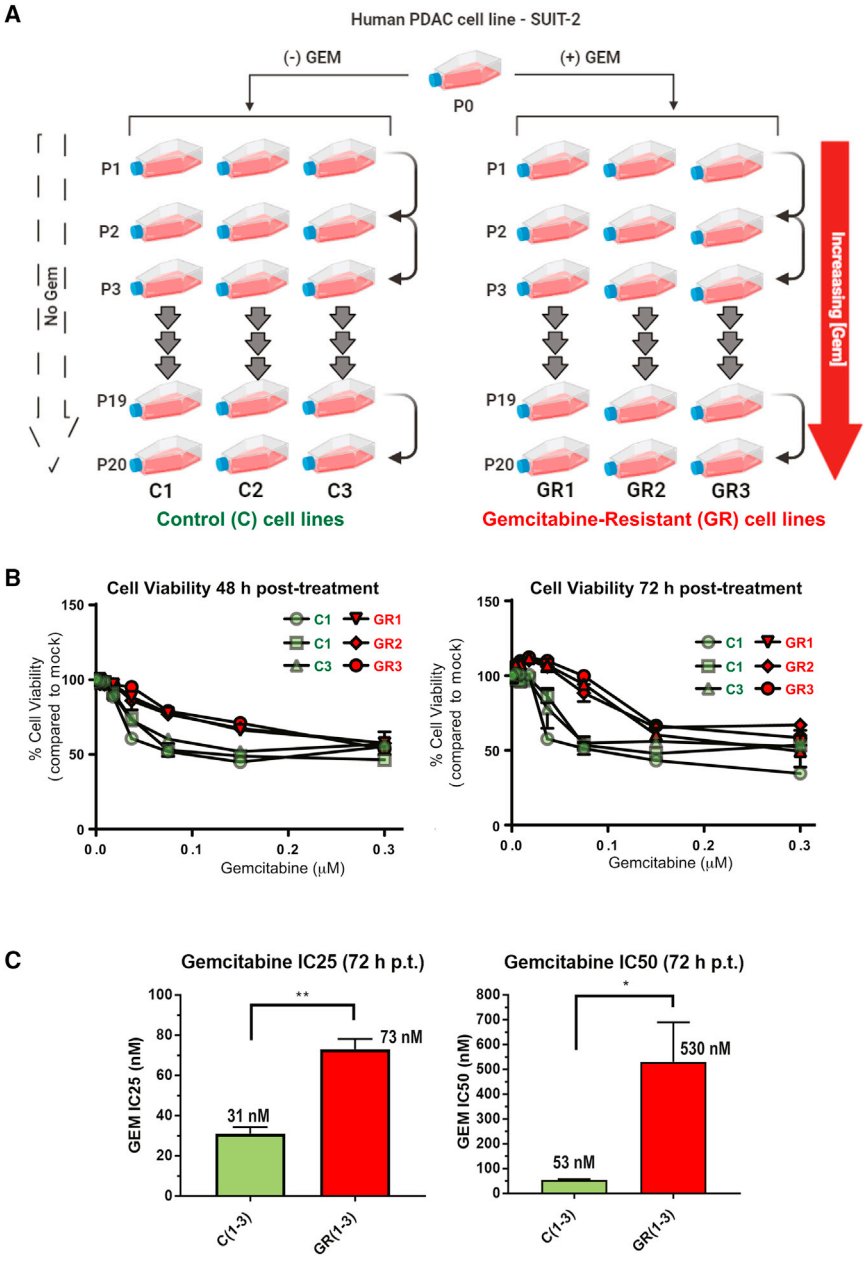

Figure 1. Experimental generation of gemcitabine-resistant (GR) SUIT-2 cells

(A) SUIT-2 cells were passaged in parallel for 20 generations in triplicate in the presence of gemcitabine (GR cells), or without gemcitabine-cultured media (C cells). Cells were exposed to an increasing concentration of gemcitabine from 100 nM (P1) to 25.6 μM (P20). (B) Cell viability of C and GR cells at different concentrations of gemcitabine. Cells were mock treated or treated with gemcitabine at concentrations ranging from 250 to 0.001 μM, and cell viability was measured at 48 and 72 h post-treatment (p.t.) by WST-8. (C) Comparing resistance of C and GR cells to gemcitabine. IC25 and IC50 values were calculated using GraphPad Prism 7.04. (B) and (C) represent results from at least three independent experiments. The data points and error bars shown represent the means and SEM of the means, respectively. Results were analyzed to determine significance using a Student's t test. *$p < 0.05$, **$p < 0.01$.

that remains unanswered is how tumor chemoresistance (inherent or acquired) may impact its responsiveness to OV therapy. As tumor chemoresistance may be one of the predictors for the success of OV therapy, understanding this could benefit the way the individualized treatment regimens for PDAC patients are rationally scheduled.

Gemcitabine (2′-deoxy-2′,2′-difluorocytidine monohydrochloride; dFdC; trade names Gemzar, Infugem) is a deoxycytidine analogue, and gemcitabine-based chemotherapy regimens are the standard of care for patients with PDAC.[24] Here, we experimentally generated human PDAC cells with increased resistance to gemcitabine and examined how the acquired phenotype affected responsiveness of PDAC cells to OV therapy. Our data show that the acquired resistance to gemcitabine can lead to cross-resistance of PDAC cells to VSV and Sendai virus (a paramyxovirus). We also show that the increased resistance of these cell lines to both gemcitabine and tested viruses correlated with upregulated levels of a subset of ISGs, resembling the interferon-related DNA damage resistance signature (IRDS), often associated with resistance of cancer cells to chemotherapy and/or radiation therapy.[25–28] Analysis of 10 different PDAC cell lines showed that, although no statistically significant correlation between chemoresistance and resistance to VSV was observed in all 10 tested PDAC cell lines, 4 PDAC cell lines most resistant to VSV were also highly resistant to gemcitabine. Moreover, the same 4 cell lines all displayed IRDS-like expression in our previous reports.[18,19,23,29] To the best of our knowledge, this is the first study to examine how experimentally acquired chemoresistance impacts the effectiveness of OV therapy.

RESULTS

Experimental generation of gemcitabine-resistant human PDAC cells

The human PDAC cell line SUIT-2[30] was used for the experimental generation of gemcitabine-resistant cells (Figure 1A). This cell line has been extensively studied in our laboratory, and SUIT-2 cells display an intermediate level of permissiveness to VSV compared with other tested PDAC cell lines.[17,18,20] Parental SUIT-2 cells were

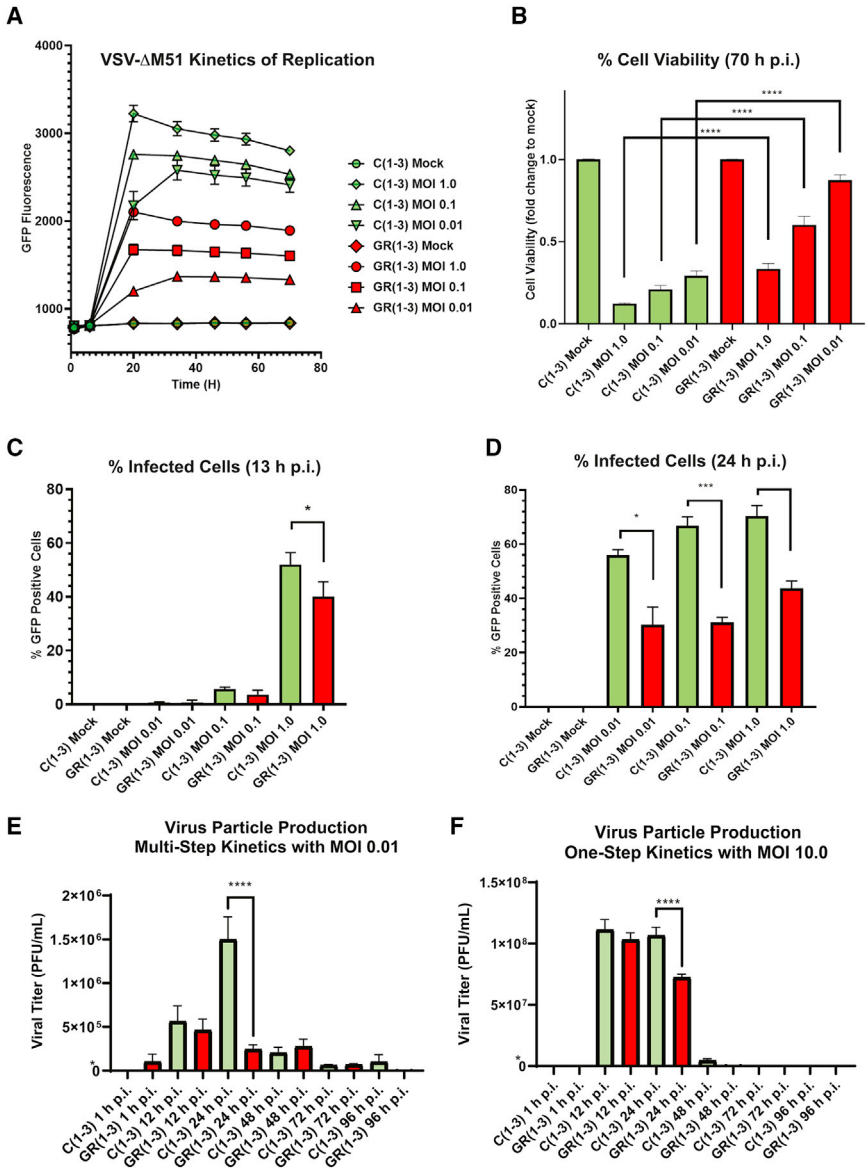

Figure 2. Viral replication kinetics

(A) C and GR cell lines were either mock treated or infected with VSV-ΔM51 at MOIs of 1.0, 0.1, or 0.01. GFP fluorescence was measured over time from 1 to 72 h p.i. Control and GR cell lines 1–3 are combined for each MOI. (B) Cell viability of C and GR cells 70 h after infection at different MOIs. Control and GR cell lines were either mock treated or infected with VSV-ΔM51 at MOIs of 1.0, 0.1, or 0.01. Cell viability was measure 70 h p.i. using a WST-8 cell viability assay. The figure represents data from three independent experiments. (C and D) Percent of infected C and GR cells to determine differences in ability of VSV to spread. Control and GR cells were infected with VSV-ΔM51 at MOIs of 1.0, 0.1, and 0.01. Samples were collected at 13 and 24 h p.i. Samples were trypsinized and the percent of GFP-positive cells was determined by using a Nexcelom Cellometer Vision fluorescent cell counting system. (E and F) Virus particle production: one step and multi-step virus kinetics in C and GR cells. Control and GR cells were infected with VSV-ΔM51 at an MOI of 0.01 (E) or MOI 10 (F). Wells were washed after initial 1-h infection and fresh media was added to all wells. Supernatant was collected at 1, 12, 24, 48, 72, and 96 h p.i. Virus titers were determined for each time point using standard plaque assay on BHK-21 cells. The data points and error bars shown represent the means and SEM of the means, respectively (some error bars are too small to be seen in the figures). Results were analyzed to determine significance using a Student's t test or one-way analysis of variance with a Sidak's multiple comparison test at a 95% confidence interval for comparison between each condition. *$p < 0.05$, **$p < 0.01$, ***$p < 0.001$, ****$p < 0.0001$. Control and GR cell lines 1–3 are combined for each MOI.

split into 6 individual flasks and passaged twenty times in parallel without gemcitabine treatment to generate three *control* ("C") cell lines, and in the presence of gemcitabine to generate three *gemcitabine-resistant* ("GR") cell lines (Figure 1A). Cells were allowed to reach approximately 100% confluence before being passaged again, and with each passage, the gemcitabine concentration was gradually increased, as conducted in previous studies.[31,32] The C cells were passaged in parallel, but without gemcitabine.

To compare the responsiveness to gemcitabine for SUIT-2 cells passaged 20 times in the presence or absence of the drug, the C cell lines (C1, C2, and C3) and the GR cell lines (GR1, GR2, and GR3) were treated with serial dilutions of gemcitabine for 48 h or 72 h, followed by a cell viability assay (Figure 1B). As expected, GR cells became more resistant to gemcitabine compared with C cells (Figure 1B), although the observed resistance of cells lines to gemcitabine was modest, with IC25 of 73 nM for GR cells compared with 31 nM for C cells, and IC50 of 530 nM for GR cells compared with 53 nM for C cells (Figure 1C). Together, our data show that the long-term exposure of SUIT-2 cells to increased concentrations of gemcitabine resulted in the increased resistance of all three SUIT-2-originated GR cell lines to the drug.

GR PDAC cells developed increased resistance to VSV-ΔM51 infection

To compare C and GR cells in their responsiveness to VSV, we compared the ability of the oncolytic VSV recombinant VSV-ΔM51 to replicate in C and GR cells (Figure 2). VSV-ΔM51 has a deletion of the methionine residue at position 51 (ΔM51) in the VSV-encoded matrix (M) protein. This mutation prevents VSV-M from binding to the Rae1-Nup98 mRNA export complex required for cellular mRNA transport and subsequent translation. Therefore, VSV-ΔM51 is not able to inhibit antiviral responses in initially

infected cells (normal or cancer) by disrupting transport and translation of cellular mRNAs for antiviral genes, which limits its replication in the neighboring normal cells but not in cancer cells as they are typically defective in antiviral responses.[33–35] In addition, the particular recombinant virus VSV-ΔM51 used in this study contains the green fluorescent protein (GFP) reporter gene inserted at position 5 of the viral genome between the VSV G and L genes, which allows for monitoring of virus replication and spread based on VSV replication-driven GFP expression.[36] GFP expression has been shown to correlate well with virus replication in VSV-ΔM51-infected cells.[36] The C and GR cells were mock infected or infected with VSV-ΔM51 at a multiplicity of infection (MOI) of 1, 0.1, or 0.01 (herein and after the MOI was calculated based on viral titer on BHK-21, a reference cell line highly permissive to VSV), and GFP expression was examined over time by measuring GFP fluorescence. As shown in Figure 2A, GR cells showed markedly lower levels of VSV-driven GFP expression compared with C cells at each tested MOI. To examine whether the different levels of GFP expression correlated with cell viability, the C and GR cell lines were infected with VSV-ΔM51 for 70 h, followed by a cell viability assay. We found that the decrease in VSV replication-dependent GFP expression in GR cells correlated with higher cell viability of GR cells, compared with C cells (Figure 2B).

While Figure 2A demonstrates higher overall GFP levels in VSV-infected C cells compared with GR cells, we also wanted to compare the percent of GFP-positive cells over time in C and GR cell lines infected with the same amounts of VSV. Cells were infected with VSV-ΔM51 at different MOIs, and the percent of GFP-positive cells was measured at 13 h post-infection (p.i.) (Figure 2C) and 24 h p.i. (Figure 2D) using a fluorescent cell counter. We found that at 13 h p.i., there were fewer GR cells infected at an MOI 1, and at 24 h p.i., there were markedly fewer GR cells infected at each MOI, compared with C cells.

To compare virus yield in C and GR cell lines, *de novo* VSV virion production was measured in C and GR cells after a low MOI infection condition (for multi-step virus growth kinetics) and a high MOI infection condition (for single-step virus growth kinetics). We found that at 24 h p.i. for both multi-step (Figure 2E) and single-step kinetics (Figure 2F), GR cell lines produced significantly fewer virus particles compared with C cell lines. Interestingly, VSV virion production did not differ between C and GR cells at 12 h p.i., suggesting that virus replication and spread were restricted at later stages. There were low or non-detectable levels of virus particles after 48 h p.i., likely due to cell death and expired virus particles, which were detectable at earlier times.

To compare the abilities of VSV-ΔM51 to initiate infections and spread to neighboring cells in C and GR cell lines, we infected cells with the same serial dilutions of VSV-ΔM51, overlaid them with agar, and then microscopically analyzed cell monolayers at 48 or 72 h p.i. to count focus-forming units (FFUs) and compare sizes of virus-induced fluorescent foci. In addition, we performed a standard plaque assay to count and compare the sizes of virus-induced plaques. In agreement with higher replication levels of VSV-ΔM51 in C cells (Figure 2), we observed markedly larger plaques (Figure 3A) and fluorescent foci (Figure 3B) in C cells, compared with GR cells. However, there was no statistically significant difference in the numbers of FFU/mL (Figure 3C) or plaque-forming units per milliliter (PFU/mL) (Figure 3A and data not shown) between C and GR cells. Our data are also in agreement with our analysis of virus yield in C and GR cells at early and later time points (Figures 2E and 2F), suggesting that VSV-ΔM51 has similar abilities to initiate infection in C and GR cells, but that virus replication and spread was restricted at later stages in GR cells.

To examine how stable the observed difference is in the permissiveness to VSV-ΔM51 between GR and C cell lines, C and GR cell lines were passaged 20 additional times in the absence of gemcitabine to generate passage 40 ("P.40") C cell lines (C1, C2, and C3) and P.40 GR cell lines (GR1, GR 2, and GR 3), and then cells were either mock treated or infected with VSV-ΔM51 at different MOIs, and GFP fluorescence was measured over time from 1 h p.i. to 72 h p.i. (Figure 4A). In addition, P.40 C and P.40 GR cells were examined for cell viability at 70 h p.i. (Figure 4B). Our data demonstrate that that GR cell lines stably maintain higher resistance to VSV compared with C cells (Figures 4A and 4B). To examine if the increased resistance of GR cells is specific to VSV-ΔM51 only, we infected C and GR cell lines with either VSV-ΔM51 or VSV-M(wt) (VSV containing a wild-type matrix (M) protein and GFP reporter gene) or a recombinant Sendai virus (SeV, a paramyxovirus) SeV-F_{mut} at different MOIs, and we measured virus replication-driven GFP fluorescence over time. Similar to VSV-ΔM51, VSV-M(wt) and SeV-F_{mut} replicated at lower levels in GR cells compared with C cells at most tested MOIs (Figure 4C).

GR cell lines exhibit increased STAT1/STAT2 antiviral signaling compared with C cell lines

Our previous studies demonstrated the major role of constitutive and/or virus-induced type I IFN antiviral responses in resistance of some PDAC cell lines to VSV and other tested OVs.[17,19,23] The observed resistance of GR cells to both VSV and SeV could suggest the same mechanism in GR cells. In the canonical type I IFN-induced signaling pathway,[37] the interaction of type I IFNs (IFN-α or IFN-β) with IFN-α receptor (IFNAR) activates the IFNAR-associated protein tyrosine kinases Janus kinase 1 (JAK1) and tyrosine kinase 2 (TYK2), which phosphorylate the cytoplasmic transcription factors signal transducer and activator of transcription 1 (STAT1) and 2 (STAT2). Phosphorylated STAT1-STAT2 heterodimer then dissociates from the receptors and recruits IFN-regulatory factor 9 (IRF9) in the cytoplasm to form a trimolecular complex called IFN-stimulated gene factor 3 (ISGF3). ISGF3 then translocates to the nucleus, where it binds to DNA sequences with so-called IFN-stimulated response elements, directly activating the transcription of a large number of antiviral ISGs.

To examine the role of type I IFN responses in resistance of GR cells to viruses, we infected C and GR cells with VSV-ΔM51 at different MOIs, where total protein was isolated at 24 (Figure 5A) and 48 h p.i. (Figure 5B), and analyzed by western blotting for major

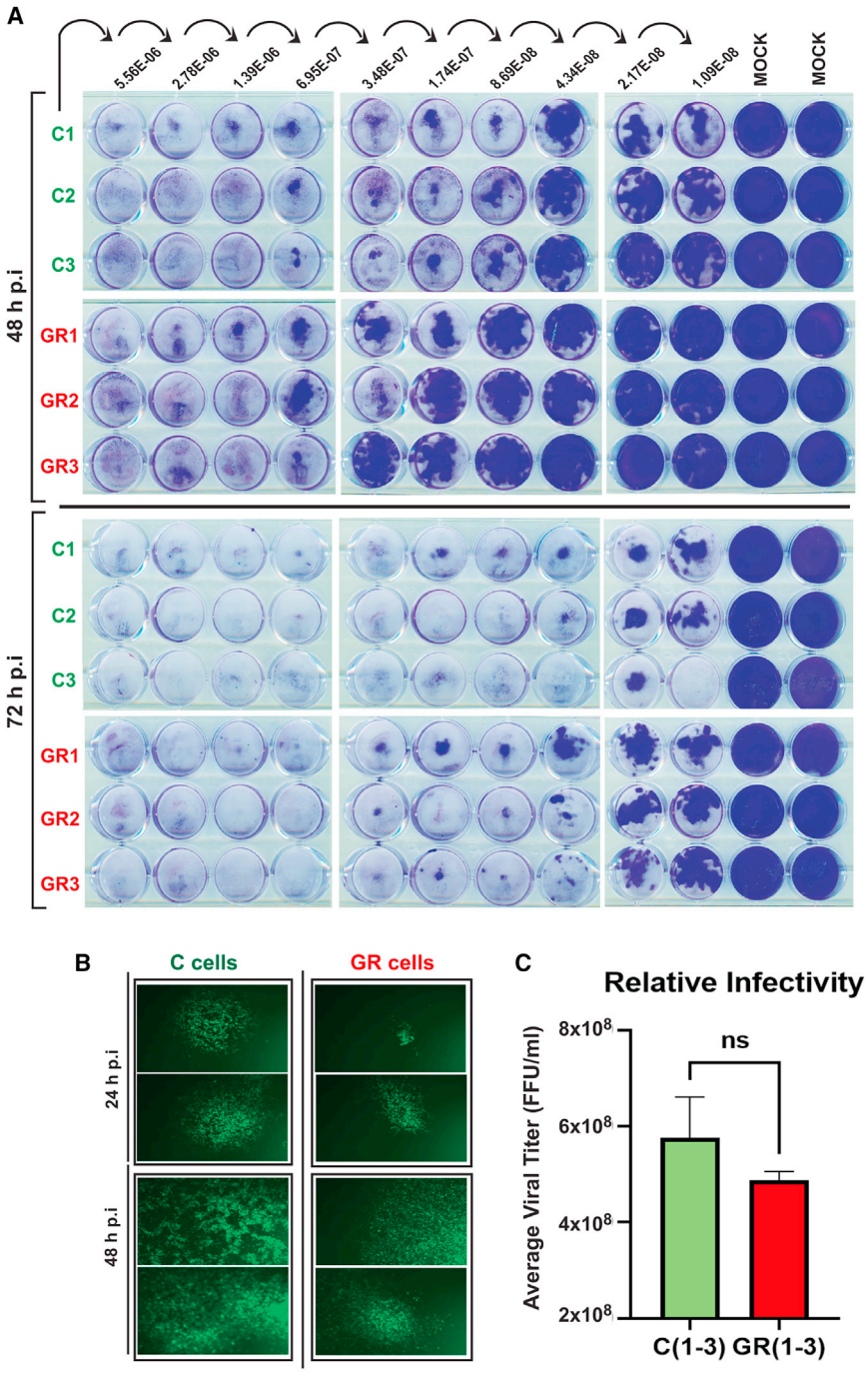

Figure 3. Relative infectivity and infection foci of VSV in C and GR cells

(A) C and GR cells were either mock treated or infected with serial dilutions of VSV-ΔM51 from 5.56×10^{-6} to 2.17×10^{-8}. Cells were fixed and stained at 48 and 72 h p.i. (B) Comparing VSV-mediated fluorescent foci in C and GR cells at 24 and 48 h p.i. Two representative foci are shown for each cell line and time point. (C) Comparing VSV titers on C and GR cells. The data points and error bars shown represent the means and SEM of the means, respectively. Results were analyzed to determine significance using the Student's t test. C and GR cell lines 1–3 are combined. ns, not significant.

modulators of type I IFN signaling: total STAT1, phosphorylated STAT1 (p-STAT1-Ser727), total STAT2, and phosphorylated STAT2 (p-STAT2-Tyr689). VSV protein accumulation was also analyzed. In agreement with our hypothesis, at both 24 and 48 h p.i., and at all tested MOIs, protein accumulation of total STAT1, p-STAT1, total STAT2, and p-STAT2 was greater in GR cells compared with C cells, which also negatively correlated with overall VSV protein accumulation. In mock-treated cells, we were unable to detect clear differences in STAT1, p-STAT1, STAT2, or p-STAT2 protein expression, in part due to the low levels of some of these proteins in uninfected cells.

To further study the role of antiviral signaling in the resistance of GR cells to VSV, we examined the effect of ruxolitinib on VSV-ΔM51 replication in GR cells (Figure 5C) and C cells (Figure 5D). Ruxolitinib ("Ruxo" in Figures 5C and 5D) is an FDA-approved drug (brand names Jakafi and Jakavi) and a selective JAK1/JAK2 kinase inhibitor that shuts down the JAK/STAT signaling axis. We hypothesized that if GR cells are more resistant to VSV due to increased antiviral signaling, then the treatment with ruxolitinib would enhance VSV replication in GR cells compared with C cells. C and GR cells were infected with VSV-ΔM51 at an MOI of 0.01, then either mock treated or treated with 10 μM or 0.02 μM ruxolitinib, and VSV replication-directed GFP expression was measured until 80 h p.i. In agreement with our hypothesis, our data showed that at both higher and lower concentrations, ruxolitinib increased VSV-ΔM51 replication in GR cells, but not in C cells (Figures 5C and 5D).

To further investigate the role of antiviral signaling in the resistance of GR cells to virus infection, we conducted a global transcriptome analysis comparing mRNA levels in uninfected C and GR cells. Our goal was to identify genes and pathways that could potentially play a role in increased resistance of GR cells to VSV. Total RNA was isolated from untreated C and GR cells, analyzed by RNA sequencing (RNA-seq) to get a global, transcript-level snapshot of gene expression, and a gene ontology (GO) analysis was performed to identify significantly enriched biological processes in GR cells compared

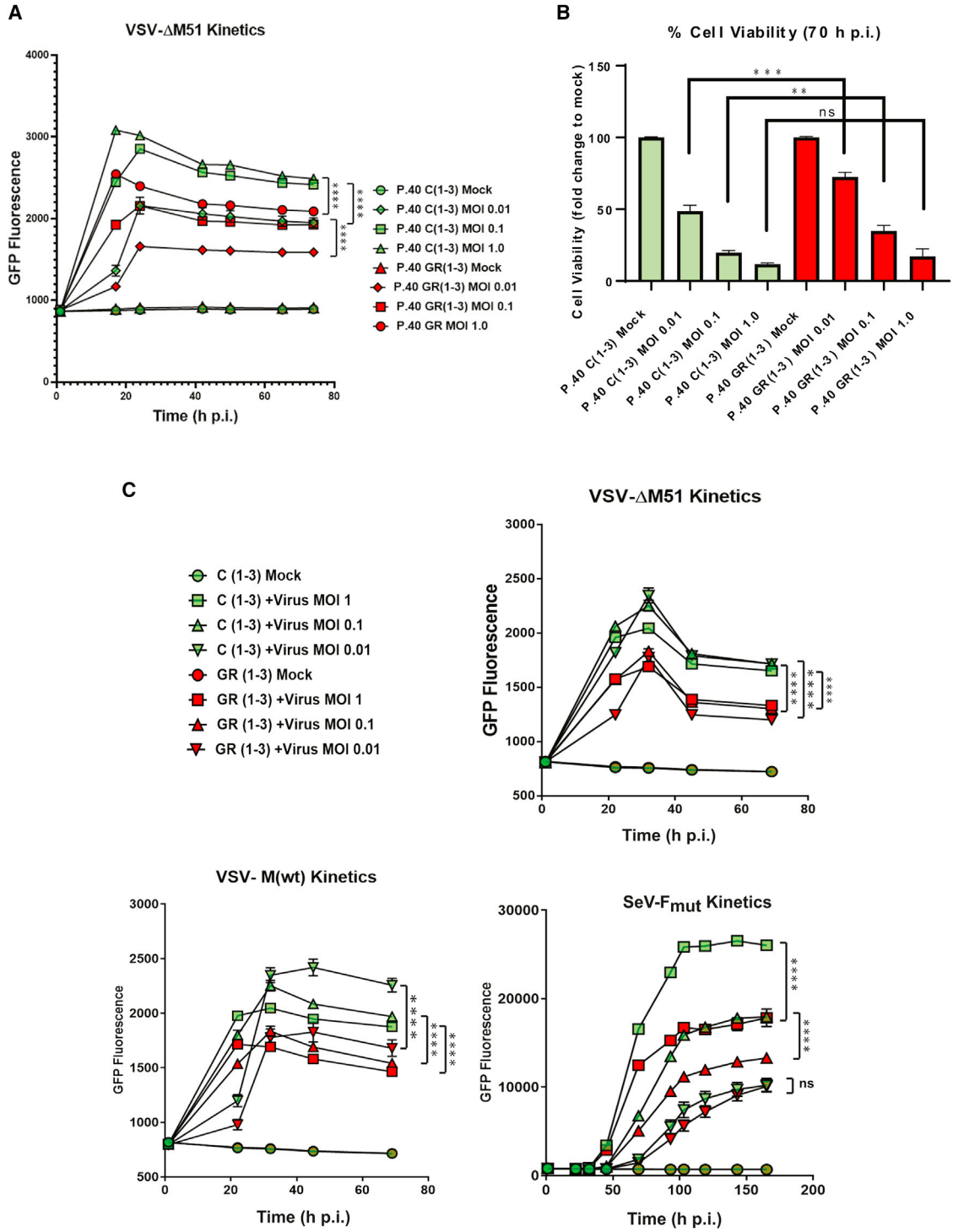

Figure 4. Replication kinetics of different viruses in C and GR cells

(A and B) GR cells maintain VSV-resistant phenotype after at least 20 additional passages in the absence of gemcitabine. (A) C and GR cell lines were passaged 20 additional times in the absence of gemcitabine to generate passage 40 (P.40) C and P.40 GR cell lines, and then viral replication kinetics based on VSV-driven GFP expression levels was examined. Cells were either mock treated or infected with VSV-ΔM51 at MOIs of 1.0, 0.1, or 0.01. GFP fluorescence was measured over time from 1 to 72 h p.i. Control and GR cell lines 1–3 are combined for each MOI. (B) Cell viability of P.40 C and P.40 GR cells 70 h after infection at different MOIs. P.40 C and P.40 GR cell lines were either mock treated or infected with VSV-ΔM51 at MOIs of 1.0, 0.1, or 0.01. Cell viability was measured 70 h p.i. using a WST-8 cell viability assay. The figure represents data from

(legend continued on next page)

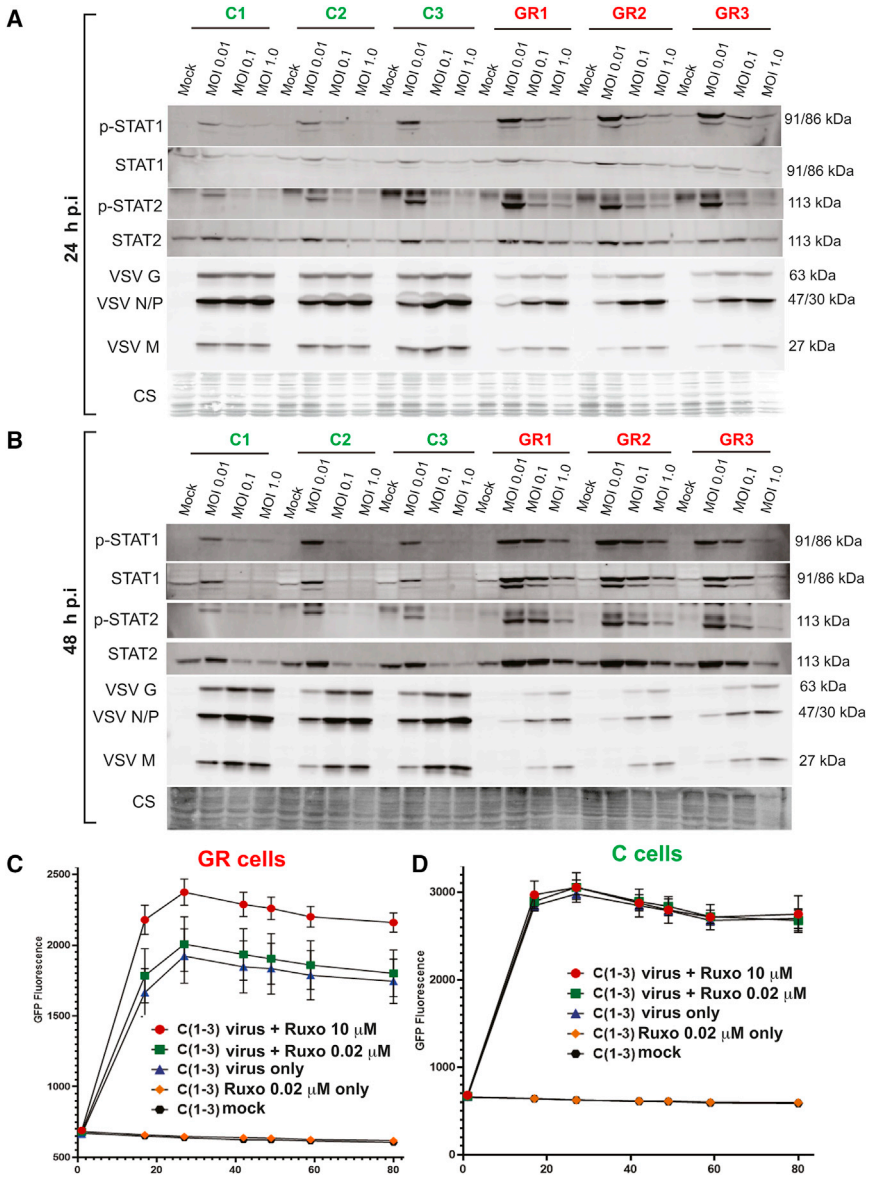

Figure 5. VSV and antiviral protein expression

(A and B) C and GR cells were either mock treated or infected with VSV-ΔM51 at MOIs of 1.0, 0.1, and 0.01. Protein sample were analyzed at 24 h p.i. (A) and 48 h p.i. (B) by western blotting for expression of phospho-STAT1 (p-STAT1), phospho-STAT2 (p-STAT2), STAT1, STAT2, and VSV proteins (G, N/P, and M). Cell line and treatment conditions are indicated above blots. Equal protein loading is indicated by Coomassie blue. (C and D) The effect of ruxolitinib on VSV-ΔM51 replication kinetics based on GFP fluorescence. C and GR cells were either mock treated, treated only with ruxolitinib, treated only with VSV-ΔM51, or treated with both VSV-ΔM51 and ruxolitinib. Cells were infected at MOI of 0.01. Ruxolitinib was added to cells after 1 h VSV incubation period. GFP fluorescence was measured from 1 to 80 h p.i. The data points and error bars shown represent the means and SEM of the means, respectively. Control and GR cell lines 1–3 are combined for each treatment.

with C cells (Figure 6A). Importantly, among the top 40 biological processes positively or negatively modified in GR cells, there were 6 processes associated with antiviral signaling, and they were all significantly upregulated in GR cells compared with C cells (Figure 6A, red text boxes). These data agree with the reduced levels of VSV-ΔM51 replication in GR cells compared with C cells (Figures 2 and 4) and with the increased expression of major antiviral signaling proteins (Figure 5). To further investigate the specific genes associated with cellular antiviral responses, we utilized the QIAGEN Ingenuity Pathway Analysis (IPA) software. Figure 6B shows some of the most enriched genes that are associated with the IPA-defined processes "Antiviral response" and "Replication of viral replicon" between uninfected C and GR cells. The list of the most significantly upregulated genes (indicated by red shapes) includes such well-known antiviral ISGs as MX1, MX2, IRF3, IFITM1, ISG15, RSAD2 (viperin), DHX58 (LGP2), IFIT1, IFITM3, IFI16, IFI44, and APOBEC3B. These data demonstrate that even in the absence of virus infection, GR cells have upregulated levels of antiviral ISGs compared with C cells. Table 1 ("Antiviral" group) shows a more comprehensive list of differentially expressed antiviral genes in GR cells compared with C cells. This analysis revealed a significant upregulation of well-known ISGs in GR cells in the absence of virus infection, such as IFITM2, where a log2 fold change of 1.88 corresponds to a 188% upregulation in GR cells compared with C cells. The canonical IFN-induced ISG expression depends on interaction of IFNs with IFN receptors. Interestingly, however, our RNA-seq data reveal that despite the upregulation of ISGs in GR cells compared with C cells, we did not observe any upregulation for type I IFN-α, type I IFN-β (Figure 6C), type II IFN-γ (Figure 6C), or type III IFN-λ (data not shown).

three independent experiments. (C) Replication kinetics of different OVs in C and GR cells. C and GR cells were either mock treated or infected with VSV-ΔM51 (A), VSV-M(wt) (B), or SeV (C) at MOIs of 1.0, 0.1, and 0.01. GFP fluorescence was measured over times ranging from 1 to 165 h p.i. The data points and error bars shown represent the means and SEM of the means, respectively (some error bars are too small to be seen in the figures). C and GR cell lines 1–3 are combined for each MOI. Results were analyzed to determine significance using the Student's t test. *p < 0.05, **p < 0.01, ***p < 0.001, ****p < 0.0001. ns, not significant.

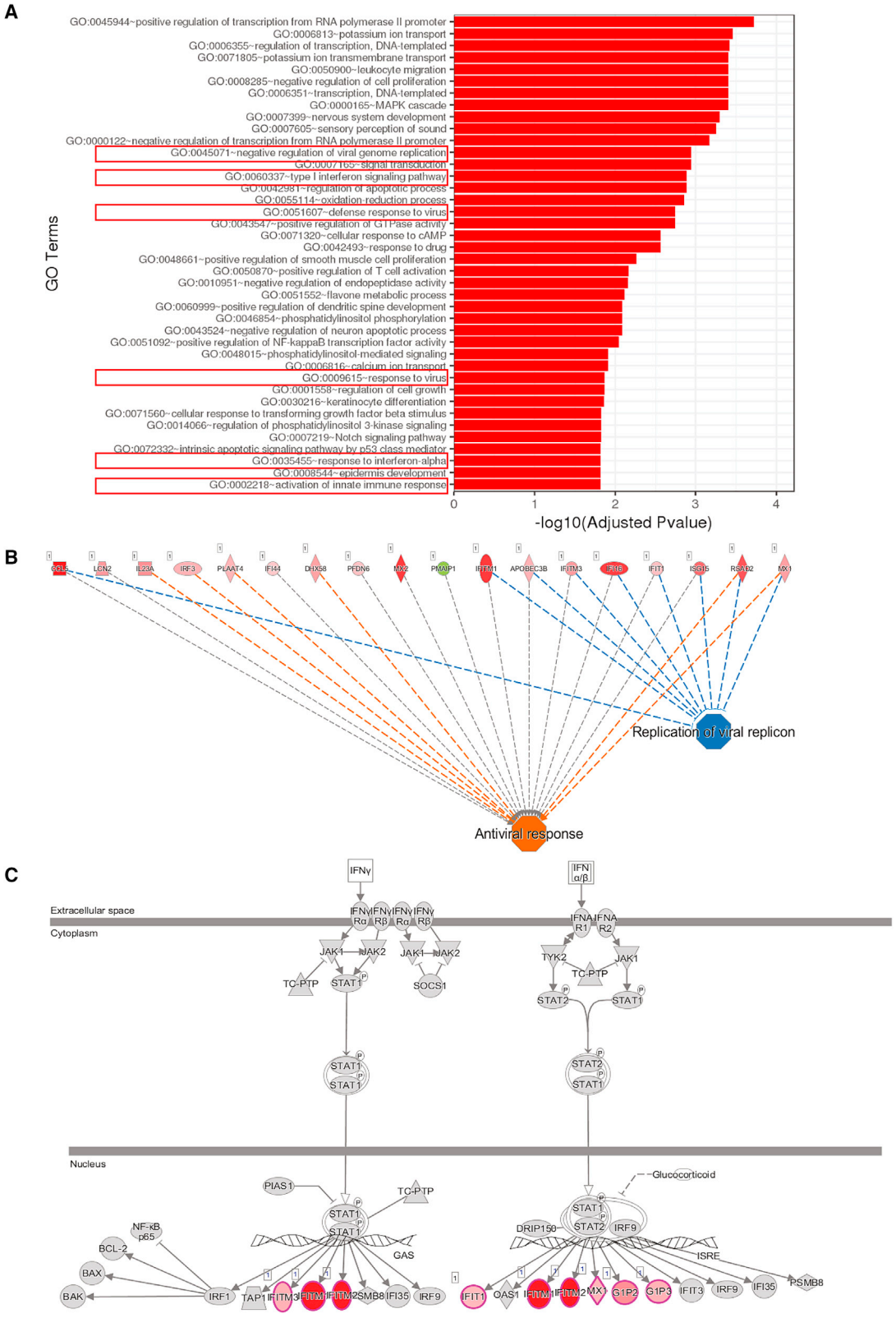

(legend on next page)

Table 2 shows genes in the gene families "cytidine deaminase," "nucleotide transporters," and deoxycytidine kinase," as genes in these groups are known to have roles in resistance to gemcitabine.[24] Complete lists of differentially expressed genes identified in this study are presented in Table S1.

Our RNA-seq data revealed a subset of ISGs that were significantly upregulated in GR cells compared with C cells at the mRNA level. To examine the protein levels of some of these ISGs at different times after infection, C and GR cells were infected with VSV-ΔM51 at MOI 0.01, total protein was collected at 1, 12, 24, and 32 h. p.i., and analysis was performed by western blotting (Figure 7A). Most antiviral proteins were expressed greater at later times post-infection, and in most cases, greater levels were observed in GR cell lines compared with C cell lines, which is consistent with our earlier experiments (Figure 5). This list includes total STAT1, p-STAT1, total STAT2, p-STAT2, MX1, MX2, IFI16, ISG15, STING, and some other ISGs. Together, our data show that GR cells have upregulated constitutive (Figure 6) and virus-inducible (Figures 5 and 7) expression of antiviral ISGs, which correlates well with the resistance of GR cells to VSV.

It is still unclear if the upregulation of these well-known antiviral ISGs plays any role in the resistance of GR cells to gemcitabine. Previous studies have shown that resistance of some cancers to chemotherapy and/or radiation therapy could be associated with so-called IRDS.[25–28] Although the exact mechanism of increased resistance of GR cell lines to gemcitabine is beyond the scope of this study, and the exact role of IRDS in resistance of some cancers to chemotherapy and/or radiation therapy is still unclear, we examined whether the ISGs overexpressed in response to VSV are also upregulated in GR cells after treatment with gemcitabine. Cells were either mock treated, infected with VSV-ΔM51 at MOI 0.01, or treated with gemcitabine at a concentration of either 5 μM or 0.1 μM. Total protein was then isolated after 32 h. As expected, STAT1, MX1, MX2, IFI16, and ISG15 were induced in all VSV-infected cell lines, and each gene upregulated greater in VSV-infected GR cells, compared with VSV-infected C cells (Figure 7B). Interestingly, the same genes were also upregulated (although to a lower level, compared with VSV-infected cells) after gemcitabine treatment, and primarily in GR cells. Our future studies will examine whether these and/or other ISGs may play a causative role in the cross-resistance of GR cells to both gemcitabine and VSV.

Analysis of cross-resistance of different human PDAC cell lines to gemcitabine and VSV

Our data show that when we experimentally generate human PDAC cells to be more resistant to gemcitabine, the cells also become more resistant to VSV, likely via upregulation of ISG expression (constitutive as well as virus-inducible). Our laboratory has previously published work demonstrating that human PDACs are heterogeneous in their resistance to VSV. To examine whether a correlation exists between gemcitabine resistance and resistance to VSV across 10 human PDAC cell lines (Table 3; Figure 8), C and GR cells were either infected with serial dilutions of VSV-ΔM51 or treated with serial dilutions of gemcitabine for 48 h. In one approach, we examined the correlation between permissiveness of PDAC cells to VSV and the effect of gemcitabine on PDAC cell viability (Figure 8A). VSV FFU were counted to obtain TCID50 (tissue culture infectious dose), which indicates the amount of virus required to infect 50% of cultured cells, and cell viability was determined for gemcitabine treated cells to obtain gemcitabine IC50 (Figure 8A). In another approach, we examined the correlation between the effect of VSV on PDAC cell viability and the effect of gemcitabine on PDAC cell viability (Figure 8B shows resistance to VSV indicated as IC50, which was obtained by measuring cell viability after 48 h instead of FFU). The analyses of these 10 different human PDAC cell lines show no statistically significant correlation between resistances to gemcitabine and VSV. Moreover, the AsPC-1 cell line was highly permissive to VSV, but it was, together with HPAF-II, the most resistant to gemcitabine among all tested PDAC cell lines. Interestingly, 4 PDAC cell lines most resistant to VSV (Hs766t, HPAF-II, CFPAC-1, and HPAC) were also among 5 PDAC cell lines (along with the aforementioned AsPC-1) most resistant to gemcitabine. Importantly, the same 4 PDAC cell lines (Hs766t, HPAF-II, CFPAC-1, and HPAC) displayed IRDS-like constitutive expression of ISGs in our previous reports.[18,19,23,29]

DISCUSSION

As VSV-based OV therapy becomes a more widely tested treatment modality in clinical trials (Clincaltrials.gov trials NCT03120624, NCT02923466, NCT03647163, and NCT03017820), it is important to understand how the efficacy of such therapy is impacted by the chemoresistant status of cancer cells. To the best of our knowledge, this is the first study to examine how experimentally acquired chemoresistance impacts the effectiveness of OV therapy. We demonstrate that long-term exposure of PDAC cells to gemcitabine results in the development of cross-resistance of PDAC cells to gemcitabine and VSV. Importantly, we generated and studied 6 independent PDAC cell lines (3 GR and 3 C), and we show that each of the 3 GR cell lines developed a similar cross-resistance phenotype to gemcitabine and VSV.

The increase in resistance to VSV correlated with upregulated levels of a subset of antiviral ISGs in each of the GR cell lines. There are several indications that the upregulation of these genes is a causative factor for resistance to VSV. First of all, the list of the upregulated ISGs includes many well-known antiviral genes, including MX1,

Figure 6. Total RNA was isolated from C and GR cells in triplicate and analyzed by RNA-seq

Significant differentially expressed genes were clustered by their gene ontology, and the enrichment of gene ontology terms was tested using Fisher exact test (GeneSCF v1.1-p2). (A) Gene ontology terms that are significantly enriched with an adjusted p value less than 0.05 in the differentially expressed gene sets in GR cells compared with C cells in the absence of virus infection. Processes relating to antiviral signaling are boxed in red. (B) Ingenuity Pathway Analysis (IPA) illustrating gene products enriched in GR cells compared with control cells in the absence of virus infection. (C) IPA conical IFNα/β and IFNγ pathways and gene products involved. Enriched genes are colored red (darker red indicates greater enrichment).

Table 1. Differentially expressed antiviral genes in GR cells compared with C cells

Gene id	Gene name	GR1 vs. C1 (log2 fold change)	GR2 vs. C1 (log2 fold change)	GR3 vs. C1 (log2 fold change)
ENSG00000130303	*BST2*	0.99*	0.79*	0.54*
ENSG00000163739	*CXCL1*	1.41*	1.44*	1.27
ENSG00000161921	*CXCL16*	0.73*	0.78*	0.87*
ENSG00000107485	*GATA3*	0.89*	0.71*	0.49*
ENSG00000204257	*HLA-DMA*	1.03*	0.94*	0.76*
ENSG00000242574	*HLA-DMB*	1.75*	1.89*	1.57*
ENSG00000179344	*HLA-DQB1*	1.27*	0.78*	0.88*
ENSG00000196126	*HLA-DRB1*	0.82*	0.76*	0.76*
ENSG00000204632	*HLA-G*	0.63	0.27	0.28
ENSG00000230795	*HLA-K*	0.76*	0.68*	0.57
ENSG00000132196	*HSD17B7*	0.46*	0.58*	0.39
ENSG00000163565	*IFI16*	1.35*	1.25*	1.14*
ENSG00000119632	*IFI27L2*	0.74*	0.61*	0.11
ENSG00000068079	*IFI35*	0.47*	0.21	−0.03
ENSG00000137965	*IFI44*	0.51*	0.47*	0.22
ENSG00000185745	*IFIT1*	0.57*	0.59*	0.48*
ENSG00000119917	*IFIT3*	0.35*	0.28	0.07
ENSG00000185885	*IFITM1*	1.39*	1.61*	1.11*
ENSG00000185201	*IFITM2*	1.88*	1.72*	1.55*
ENSG00000142089	*IFITM3*	0.82*	0.65*	0.41*
ENSG00000126456	*IRF3*	0.67*	0.58*	0.38*
ENSG00000117595	*IRF6*	0.56*	0.48*	0.39*
ENSG00000187608	*ISG15*	1.12*	0.87*	0.61*
ENSG00000078081	*LAMP3*	0.84*	0.97*	0.78*
ENSG00000168961	*LGALS9*	1.58*	1.39*	0.81*
ENSG00000167656	*LY6D*	0.86*	0.63*	0.39
ENSG00000160932	*LY6E*	0.93*	0.81*	0.53*
ENSG00000157601	*MX1*	0.80*	0.62*	0.12
ENSG00000183486	*MX2*	1.38*	1.62*	1.51*
ENSG00000183486	*MX2*	1.38*	1.62*	1.51*
ENSG00000135114	*OASL*	0.48*	0.4	0.08
ENSG00000178685	*PARP10*	0.77*	0.61*	0.44*
ENSG00000134321	*RSAD2*	1.24*	1.04	0.77
ENSG00000196154	*S100A4*	1.00*	0.84*	0.64*
ENSG00000197249	*SERPINA1*	2.42*	2.06*	2.15*
ENSG00000188488	*SERPINA5*	0.65*	0.58*	0.60*
ENSG00000170099	*SERPINA6*	2.57*	2.54*	2.35*
ENSG00000167711	*SERPINF2*	1.15*	0.94*	0.84*
ENSG00000115415	*STAT1*	0.08	0.22	0.29
ENSG00000126561	*STAT5A*	0.86*	0.62*	0.43
ENSG00000166888	*STAT6*	0.64*	0.65*	0.68*
ENSG00000204610	*TRIM15*	0.68*	0.79*	0.56*
ENSG00000112343	*TRIM38*	0.51*	0.47*	0.44*
ENSG00000132481	*TRIM47*	0.44*	0.41*	0.23
ENSG00000169871	*TRIM56*	0.38*	0.30*	0.18
ENSG00000141569	*TRIM65*	0.38*	0.34*	0.32*
ENSG00000146054	*TRIM7*	0.38*	0.40*	0.28
ENSG00000027697	*IFNGR1*	−0.01	0.06	0.1
ENSG00000142166	*IFNAR1*	0.01	0.07	0.11
ENSG00000159110	*IFNAR2*	0.2	0.36*	0.3
ENSG00000159128	*IFNGR2*	0.32*	0.37*	0.21
ENSG00000182393	*IFNL1*	ND	ND	ND
ENSG00000183709	*IFNL2*	ND	ND	ND
ENSG00000184995	*IFNE*	−0.54	−0.27	−0.92
ENSG00000185436	*IFNLR1*	0.08	0.11	0.17
ENSG00000197110	*IFNL3*	ND	ND	ND
ENSG00000238271	*IFNWP19*	−0.89	−0.67	−0.13

Gene log2 fold change values compared with C cells. Values denoted with an asterisk indicate a p value of less than 0.05.

MX2, IRF3, IFITM1, ISG15, RSAD2 (viperin), DHX58 (LGP2), IFIT1, IFITM3, IFI16, IFI44, and APOBEC3B. Secondly, GR cells not only became more resistant to VSV but also to another NNS RNA virus, SeV, suggesting a more general virus restriction mechanism. Thirdly, treatment of C and GR cells with a JAK1/JAK2 inhibitor ruxolitinib stimulated virus replication in GR cells but not C cells, suggesting a greater role of antiviral signaling in GR cells. These results are supported by our previous study demonstrating specific downregulation of hundreds of ISGs by ruxolitinib in PDAC cells resistant to VSV.[19]

The role of type I IFN signaling in cancer is multifaceted and has been comprehensively reviewed elsewhere.[38–41] The efficacy of many different therapeutic strategies against cancer, such as chemotherapy, radiotherapy, immunotherapies, and OV therapy, often depend on intact or at least partially active type I IFN signaling in cancer cells, for both direct (tumor cell inhibition) and indirect (antitumor immune response) effects.[41] However, despite the fact that type I IFN responses are generally considered antiproliferative, antiangiogenic, and proapoptotic, it has been observed that chronic inflammation and prolonged type I IFN stimulation may lead to chemoresistance, as detailed in the case of chronic viral infection.[42]

It is important to note that continued exposure to gemcitabine may result in numerous consequences (including upregulation of ISGs), some not directly affecting resistance to virus or even to gemcitabine. However, multiple previous studies have demonstrated the association

Table 2. Expression of other genes with known roles in resistance to gemcitabine in GR cells compared with C cells

Group	Gene id	Gene name	GR1 vs. C1 (log2 fold change)	GR2 vs. C1 (log2 fold change)	GR3 vs. C1 (log2 fold change)
Cytidine deaminases	ENSG00000179750	*APOBEC3B*	0.66*	0.59*	0.68*
	ENSG00000128394	*APOBEC3F*	−0.09	0.01	−0.18
	ENSG00000243811	*APOBEC3D*	0.73*	0.68*	0.56*
	ENSG00000244509	*APOBEC3C*	0.42*	0.45*	0.27
	ENSG00000158825	*CDA*	0.05	−0.06	−0.16
	ENSG00000102543	*CDADC1*	−0.05	−0.22	−0.01
Nucleoside transporters	ENSG00000076685	*NT5C2*	−0.38	−0.16	0.09
	ENSG00000111696	*NT5DC3*	−0.39*	−0.34	−0.15
	ENSG00000122643	*NT5C3A*	0.13	0.13	0.16
	ENSG00000125458	*NT5C*	0.74*	0.45	0.27
	ENSG00000135318	*NT5E*	−0.58*	−0.45*	−0.38*
	ENSG00000141698	*NT5C3B*	0.54*	0.38*	0.25
	ENSG00000168268	*NT5DC2*	0.32*	0.23	0.15
	ENSG00000178425	*NT5DC1*	−0.01	0.09	0.07
	ENSG00000205309	*NT5M*	0.57	−0.13	−0.27
Deoxycytidine kinase	ENSG00000156136	*DCK*	−1.01*	−0.91*	−0.66*
Thymidylate synthase	ENSG00000176890	*TYMS*	−0.19	−0.11	−0.13

Gene log2 fold change values compared with C cells. Values denoted with an asterisk indicate a p value of less than 0.05.

(including causative correlation) between upregulation of some ISGs and resistance of cancers cells to chemotherapy and/or radiotherapy. An IRDS was initially described by Weichselbaum et al. across 34 different cancer cell lines, in which a subset of 36 ISGs were significantly upregulated and conferred resistance to both chemotherapy and radiotherapy.[25] A similar expression signature consisting of 8 IRDS genes—STAT1, IFI44, IFIT3, OAS1, IFIT1, ISG15, MX1, and USP18—was also shown to predict poor prognoses in glioblastoma patients post-radiotherapy.[43] Other studies have demonstrated that the upregulation of STAT1 and other ISGs included in the IRDS signature are also upregulated in doxorubicin-resistant cells.[44] Multiple studies implicate IRDS in the resistance to chemotherapy by the acquisition of stemness features, which is understood to contribute to therapy resistance.[45–47] Interestingly, we show that many of the previously reported IRDS genes are also upregulated here in GR cells. One of the ISGs identified in our study, IFITM1, has been shown previously to be not only involved in cellular defense against West Nile virus and Dengue virus,[48] but is also involved in colorectal cancer progression[49] and radioprotection.[50]

Although the previous data support the notion that the IRDS is an inherent mechanism of resistance to chemotherapy and/or radiotherapy across a multitude of human cancers, it is still unclear how IRDS protects against radiotherapy and/or chemotherapy. Under normal circumstances, the type I IFN pathway sends a cytotoxic signal either in response to virus infection, DNA damage, or to IFNs. However, it has been speculated that the IRDS-positive cells demonstrate constitutive activation of the type I IFN pathway, which may reflect a history of chronic stimulation. This chronically stimulated state may select for the failure to transmit a cytotoxic signal and instead results in pro-survival signals mediated by STAT1 and other IRDS genes.[25]

Our results clearly demonstrate an upregulation of antiviral ISGs in GR cells, and these results are consistent with the IRDS signature. However, the underlying mechanisms of this IRDS signature development in GR cells remain unclear. Here, we describe multiple possibilities that could have led to the observed IRDS signature in our GR cells.

The role of the STING pathway in promoting IFN-mediated resistance to chemotherapy has been previously demonstrated for breast cancer regrowth after chemotherapy and activation of the STING pathway in response to the chemotherapy.[51] Interestingly, many of the upregulated genes identified in that response to chemotherapy overlapped with IRDS. Moreover, STING silencing after chemotherapy re-sensitized the cancer cells to chemotherapy.[51] Therefore, the STING/IFN/STAT1 pathway may act as a cellular mechanism for cancer cell chemoresistance and survival after chemotherapy treatment. Our data are consistent with this hypothesis, as we observed increased STING expression in GR cells as early as 1 h p.i. and up to 32 h p.i.

The role of type I IFN signaling in treatment resistance may be due at least in part to the activation of signaling downstream of type I IFN, driven by unphosphorylated STAT1 and unphosphorylated ISGF3

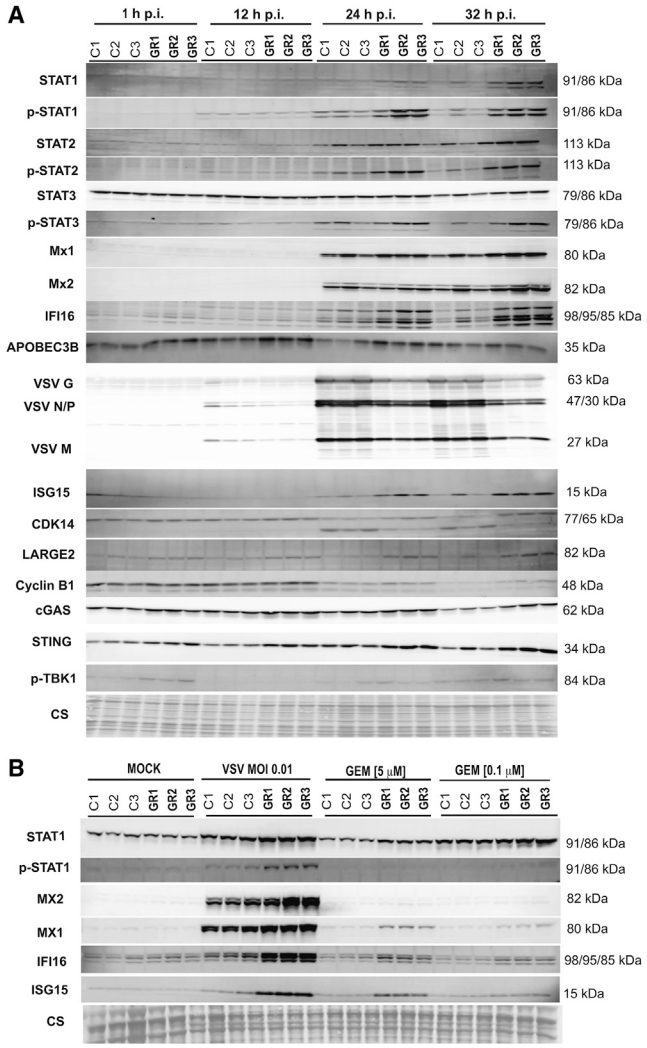

Figure 7. Time course expression of antiviral proteins in C and GR cells after VSV infection

(A) C and GR cells were infected with VSV-ΔM51 at MOI 0.01. Protein samples were collected at 1, 12, 24, and 32 h p.i. and analyzed by western blotting. Cell lines and time points are indicted above the blots. Equal protein loading is indicated by Coomassie blue. (B) C and GR cells were either mock treated, infected with VSV-ΔM51, or treated with 5 μM gemcitabine or 0.1 μM gemcitabine. Protein samples were collected after 32 h and analyzed by western blotting for expression of ISGs. Cell lines and time points are indicted above the blots. Equal protein loading is indicated by Coomassie blue.

activated upon continuing exposure, as genes upregulated by unphosphorylated STAT1 overlap with those in IRDS.[52] Our study shows greater unphosphorylated STAT1 expression after virus infection, and also after gemcitabine treatment.

Intriguingly, although we found a group of upregulated ISGs in uninfected GR cells, we did not observe any significant upregulation of type I, type II, or type III IFNs in these GR cells. This suggests that the upregulation of ISGs in GR cells may occur independently of IFNs. One possible mechanism could be an IFN-independent, but STAT-dependent ISG expression in GR cells. Although we show greater STAT1 and STAT2 expression in GR cells after infection and treatment with gemcitabine, we do not observe differences in expression in the absence of infection or treatment, as well as at the mRNA level. However, as shown in Table 1, we see significant upregulation of STAT5A and STAT6 mRNA in GR cells in the absence of infection or treatment. STAT5A is activated by various cytokines and other factors including members of the IL-3 family (IL-3, IL-5, and GM-CSF), the IL-2 family (IL-2, IL-7, TSLP, IL-9, IL-15, and IL-21), growth hormone, Epo (erythropoietin), and Tpo (thrombopoietin).[53] Intriguingly, recent studies show that STAT5A is vital for the development of various cancers and also plays a role in chemoresistance in breast cancer.[53,54] STAT6 has been shown to also play a significant role in carcinogenesis and in the early development of colon cancer.[55,56] STAT6 function has also been related to cancer cell survival and drug resistance.[57] Moreover, it has been previously shown that STAT5A and STAT5B form a complex with CrkL, resulting in translocation to the nucleus and subsequent ISG gene transcription.[58] Another previous study showed a probable role for STAT6 and ISG upregulation, as they reveal the formation of an ISGF3-like complex involving STAT6.[59] Our future studies will examine the roles of STAT5A and STAT6 in the cross-resistance phenotype and upregulation of ISGs in GR cells.

Another possible mechanism for the IFN-independent upregulation of ISGs in GR cells could be via interferon regulatory factor 3 (IRF3), as it was shown recently for upregulation of multiple ISGs, including IFIT1, IFIT2, IFIT3, ISG15, CXCL10, MX1, and MX2 in the context of human cytomegalovirus infection.[60] Indeed, another study using a tetracycline-induced expression system demonstrated an IFN-independent, IRF3-dependent upregulation of ISGs IFIT2, IFIT3, ISG15, and RSAD2 (viperin).[61] The same study demonstrated that IFIT1 upregulation can be induced directly by the expression of constitutively active IRF3. IRF3 may contribute to the upregulation of ISGs in GR cells, as our RNA-seq data reveals a significant upregulation of IRF3 in the absence of gemcitabine treatment or virus infection. However, further studies are needed to uncover the full role of IRF3.

Altogether, the cross-resistance phenotype to both chemotherapy and VSV is likely multifactorial, with no single gene or protein responsible, rather being the result of contributions from many of the aforementioned proteins. To examine this further in the future, studies need to be done by knocking out specific IRDS genes and potential upstream mediators one by one, as well as in combination, to help elucidate the importance of particular genes in this complex cross-resistant phenotype and to identify promising targets for future therapeutics. Similar studies were performed by Khodarev et al., where they used shRNA to suppress STAT1, which re-sensitized ionizing radiation (IR)-resistant squamous cell carcinoma cells to IR.[62]

Although our study mainly focused on the potential role of the observed IRDS in GR cells, it should be noted that many additional

Table 3. Human PDAC cell lines used in this study

Cell line	Origin	Chemo or radiation therapy
HPAF-II (ATCC: CRL-1997)	1982, metastasis (ascites), male, 44 years	NA
AsPC-1 (ATCC: CRL-1682)	1982, metastasis (ascites), female, 62 years	chemo and radiation
Capan-2 (ATCC: HTB-80)	1986, primary, male, 56 years	chemo
CFPAC-1 (ATCC: CRL-1918)	1990, metastasis (liver), male, 26 years	NA
MIA PaCa-2	1977, primary, male, 65 years	NA
SUIT-2	1987, primary and metastasis (lymph node), male, 73 years	NA
Capan-1 (ATCC: HTB-79)	1974, metastasis (liver), male, 40 years	chemo, 5-FU (resistant)
HPAC (ATCC: CRL-2119)	1985, primary, female, 64 years	NA
T3M4	1978, metastasis (lymph node), male, 64 years	NA
HS766t	1973, metastasis (lymph node), male, 64 years	NA

The catalog number of cell lines sold by ATCC are indicated beside the cell line name. Cell lines with "chemo" and/or "radiation" indicate treatments administered to the patient. The specific treatments are listed if information is available.

PDAC mechanisms of resistance to gemcitabine have been described.[24] Among the proteins shown to be important in resistance to gemcitabine are nucleotide transporters, deoxycytidine kinase, cytidine deaminases, ribonucleotide reductase, and thymidylate synthase. Each of these proteins act on some level to restrict gemcitabine entry and/or metabolism in the cell. Our RNA-seq analysis (Table 2) reveals that some of these genes are differentially expressed in GR cells. It is possible that at least some of these genes are involved not only in gemcitabine resistance but also in VSV resistance.

Our study here, using an experimental evolution approach, demonstrated that the prolonged exposure to gemcitabine can lead to cross-resistance of at least some PDACs to gemcitabine and oncolytic virotherapy. It is unclear if this observation can be applied to all (or most) other PDAC cell lines. To begin investigating this important question, we examined the relationship between chemoresistance and resistance to VSV-based OV therapy across a panel of 10 human PDAC cell lines. Overall, we show that there is no statistically significant correlation between resistance to gemcitabine and resistance to VSV, and PDAC cell line AsPC-1, while being one of the most GR tested PDAC cell lines, was very permissive to VSV. On the other hand, 4 PDAC cell lines most resistant to VSV (HPAF-II, Hs766t, CFPAC-1, and HPAC) were also highly resistant to gemcitabine. Intriguingly, our previous studies demonstrated that HPAF-II, Hs766t, CFPAC-1, and HPAC were also the most resistant to VSV and displayed strong IRDS phenotypes.[18,19,23,29] The lack of direct correlation between resistance to gemcitabine and VSV is not surprising, as the resistance of different PDACs to chemotherapy can occur through alternative mechanisms (other than upregulation of ISGs and/or IRDS) and due to the different treatment histories of the patients from which the cells were initially cultured.

Overall, our study shows no simple correlation between resistance to chemotherapy and resistance to VSV, indicating that at least in some patients, GR tumors can be successfully treated with VSV-based therapy. Also, even in those cases where chemoresistance enhances resistance to VSV-based therapy, chemoresistance might not prevent effective OV therapy, as our VSV treatments of GR cells were still quite effective. Also, our study was mainly focused on VSV-based OV therapy, and some tumors cross-resistant to gemcitabine and VSV could be much more permissive to other OVs, especially those that are not as sensitive to type I IFN responses as VSV-ΔM51. Lastly, the GR cells generated in this study were done so using gemcitabine only. It is important to mention that although gemcitabine monotherapy is used clinically, gemcitabine is also commonly used in combination with other chemotherapeutics such as 5-FU, nab-paclitaxel, cisplatin, oxaliplatin, etc. Hence, further studies are needed to determine if resistance to these combinations also leads to increased resistance to VSV infection. In conclusion, our study highlights a possible interaction between two different therapies that should be considered in the future for the development of more rational and individualized treatment regimens, as well as for prescreening of patients.

MATERIALS AND METHODS

Virus and cell lines

The recombinant virus VSV-ΔM51 was previously described,[36] in which the methionine at amino acid position 51 of the matrix protein is deleted and the GFP open reading frame (ORF) is inserted at position 5 of the viral genome (between VSV G and L genes). VSV-M(wt) is similar to VSV-ΔM51 (and contains the GFP ORF inserted at the same position) but has wild type M.[63] The recombinant Sendai virus SeV-GFP (SeV-GFP-F_{mut}), as described previously,[64] has the GFP ORF at position 1 of the viral genome and a mutation in the cleavage site of the fusion (F) protein, allowing F activation and production of infectious particles in cells without acetylated trypsin added to the medium. Baby hamster kidney fibroblast cells BHK-21 (ATCC CCL-10) were used to grow virus and to determine titers. Viral titers were determined by adding serial dilutions of a virus to BHK-21 cells using an agar overlay followed by calculating either FFU/mL or PFU/mL. To count PFUs, cells were fixed and stained with crystal violet. To count FFUs, VSV-encoded GFP fluorescent foci were quantified using fluorescent microscopy. The human PDAC cells used in this study were SUIT-2,[30] HPAF-II,[65] AsPC-1,[66] Capan-1,[67] Capan-2,[68] CFPAC-1,[69] MIA PaCa-2,[70] HPAC,[71] T3M4,[72] and HS766t.[73] The human origin of all tested PDAC cells lines was confirmed as previously described.[19] SUIT-2, MIA PaCa-2, HS766t, HPAC, CFPAC-1, and Capan-1 cells were maintained in Dulbecco's modified Eagle's medium (DMEM [Corning, 10-013-CV]). Capan-2, AsPC-1, and T3M4 cells were maintained in Roswell Park Memorial Institute (Corning, 10-040-CV) 1640 medium. HPAF-II and BHK-21 cells were maintained in Minimum Essential Medium (Corning 10-010-CV). All cell growth media were supplemented with 10% fetal bovine

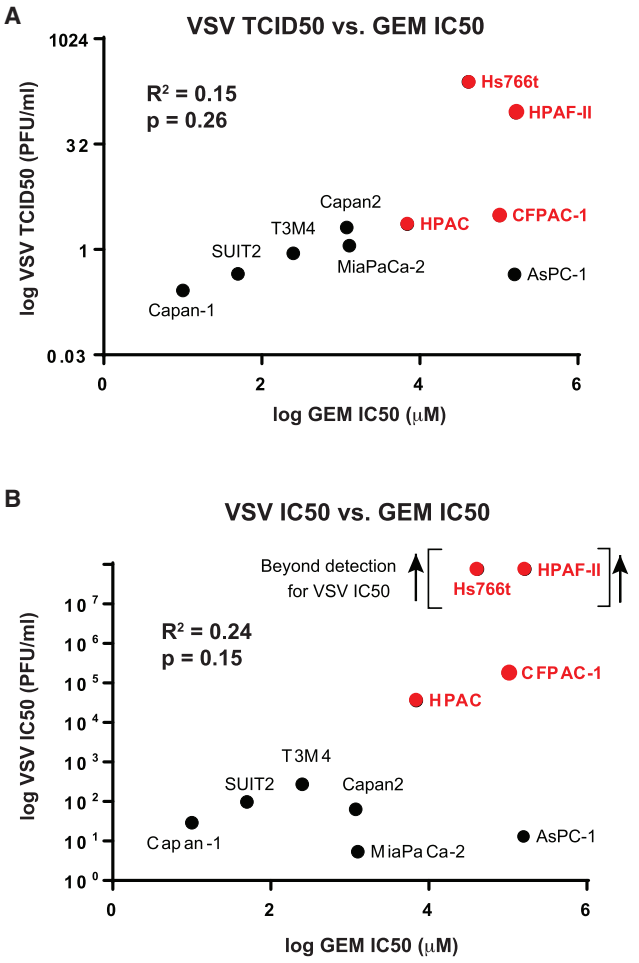

Figure 8. Human PDAC cell cross-resistance to gemcitabine and VSV-ΔM51

(A and B) Cell lines were either infected with serial dilutions of VSV-ΔM51 from 0.01 to 0.00006 PFU/mL. GFP-based FFU were counted at 24 h p.i. to calculate TCID50 values. A cell viability assay was performed at 120 h p.i. to calculate IC50 values. Separately, cell lines were treated with serial dilutions of gemcitabine at concentrations of 1,000–0.008 μM. At 120 h p.i., a cell viability assay was performed to calculate IC50 values.

serum (FBS [Gibco]), 4 mM L-glutamine, 900 U/mL penicillin, 900 μg/mL streptomycin, and 1% nonessential amino acids. HPAF-II and BHK-21 cells were additionally supplemented with 17.5% glucose. Cells were kept in a 5% CO_2 atmosphere at 37°C. For all experiments, cells were kept no more than 15 passages (except for C and GR cell lines, which were specially passaged as described below). All described experiments were approved by the University of North Carolina at Charlotte Institutional Biosafety Committee (IBC).

Generation of GR SUIT-2 cells

To select for GR SUIT-2 cells, 6 T75 cell culture flasks were independently passaged in parallel for 20 passages. 3 flasks were cultured without the presence of gemcitabine (Selleck, S1714), while 3 flasks were cultured with increasing concentrations of gemcitabine. The concentration of gemcitabine ranged from 100 nm at passage 1 to 25.6 μM at passage 20. Each passage of SUIT-2 cells was grown to 100% confluence before the next passage. At each passage, 1/3 cells were used for the next immediate passage, 1/3 cells were frozen for protein/RNA, and 1/3 cells were frozen for future cell culture.

Virus replication kinetics

For all experiments, MOI was calculated by determining the titer of viruses using standard plaque assays on BHK-21 cells in 24- or 12-well plates. For virus replication kinetics experiments, cells were seeded into 96-well plates. Virus dilutions were prepared in DMEM with 0% FBS. Cells were washed once with PBS, followed by the addition of virus for 1 h at 37°C. Virus-containing medium was aspirated, and fresh DMEM with 5% FBS was added back to cells and then incubated at 37°C in 5% CO_2 for the duration of the experiment. Virus-encoded GFP fluorescence was measured at different times over a 72-h time course using a fluorescence multiwall plate reader. GFP fluorescence was read at 485/530 nm.

Cell viability assay

For cell viability assays in a 96-well plate layout, cells were infected at either MOI 1, 0.1, or 0.01. Each cell line was also mock treated (negative control). At 70 h p.i., WST-8 (Dojindo, CK04) was added to each well for 4 h at 37°C in 5% CO_2, then read using a multi-well plate reader at 450 nm. Results are expressed as fold change compared with mock treatment.

RNA isolation, RNA-seq analysis, and gene expression analysis

Three biological repeats were used for each treatment condition for RNA-seq. SUIT-2-C1, SUIT-2-GR1, SUIT-2-GR2, and SUIT-2-GR3 cell lines were seeded into 12-well plates (0.4×10^6 cells per well) in DMEM containing 10% FBS. After 8 h, cellular RNA was isolated with TRIzol (Life Technologies) according to the manufacturer's protocol. The RNA samples were then subjected to DNAse treatment (Invitrogen TURBO DNA-free) and sent to GeneWiz for RNA sequencing. Sequence reads were trimmed to remove possible adapter sequences and nucleotides with poor quality using Trimmomatic v.0.36. The trimmed reads were mapped to the *Homo sapiens* GRCh38 reference genome available on ENSEMBL using the STAR aligner v.2.5.2b. The STAR aligner is a splice aligner that detects splice junctions and incorporates them to help align the entire read sequences. BAM files were generated as a result of this step. Unique gene hit counts were calculated by using feature Counts from the Subread package v.1.5.2. The hit counts were summarized and reported using the gene id feature in the annotation file. Only unique reads that fell within exon regions were counted. Since a strand-specific library preparation was performed, the reads were strand-specifically counted. After extraction of gene hit counts, the gene hit counts table was used for downstream differential expression analysis. Using DESeq2, a comparison of gene expression between the customer-defined groups of samples was performed. The Wald test was used to generate p values and log2 fold changes. Genes with an adjusted p value <0.05 and absolute log2 fold change >1 were called differentially expressed

genes for each comparison. A GO analysis was performed on the statistically significant set of genes by implementing the software GeneSCF v.1.1-p2. The goa_human GO list was used to cluster the set of genes based on their biological processes and determine their statistical significance. A list of genes clustered based on their gene ontologies was generated.

Plaque assay

12-well plates were seeded with SUIT-2 (GR1-GR3) and SUIT-2 (C1-C3) for about 90% confluence. The first column was infected at an MOI of 0.01, and then 2-fold serial dilutions were used to infect the remaining columns (down to MOI 0.000019). Each cell line was also mock treated (control). 1 h after infection, virus was aspirated and wells were overlayed with 2% Bacto agar (Difco Lactobacilli MRS Agar – 288210) with 5% FBS DMEM. After 72 h, formalin was added to fix cells for 4 h. After fixation, agar was removed and cells were stained with crystal violet stain solution (2% crystal violet in methanol).

Nexcelom cell counting

Cells were seeded in 24-well plates for 95% confluence. Cells were infected with VSV-ΔM51 at MOIs of 0.01 or 1 or mock infected for 13 and 24 h. After infection, cells were washed with PBS and trypsinized. Cells were then put in cell counting chambers (Nexcelom Cellometer SD100) and percent GFP-positive cells were counted using a fluorescent cell counter (Nexcelom Cellometer Vision). Calibration was performed per the manufacturer's protocol and the percent of GFP-positive cells was determined.

Western blot analysis

Cells were seeded into 12-well plates at 95% confluence. Medium was removed and cells were washed once with PBS. Virus was then added at MOIs of 0.01, 0.1, or 1 in 0% FBS medium and incubated for 1 h at 37°C. After 1 h of incubation, the medium was removed, and 5% FBS-containing medium was added to the cells. Cells were then lysed and total protein was isolated 1–48 h p.i. using buffer exactly as described previously.[74] Total protein was separated by electrophoresis on 10%–15% SDS-PAGE gels and electroblotted onto polyvinyl difluoride membranes. Membranes were blocked by using 5% nonfat powdered milk or BSA in TBS-T (0.5 M NaCl, 20 mM Tris [pH 7.5], 0.1% Tween 20) for 1 h at room temperature. Membranes were then incubated in TBS-T with 5% BSA or milk with 0.02% sodium azide and a 1:5,000 dilution of rabbit polyclonal anti-VSV antibodies (raised against VSV virions), a 1:1,000 dilution of rabbit anti-phospho-STAT1 (catalog number 9177S, clone p-S727, Cell Signaling), a 1:1,000 dilution of rabbit anti-STAT1 (catalog number 14994T, clone D1K9Y, Cell Signaling), a 1:1,000 dilution of rabbit anti-phospho-STAT2 (catalog number 600-401-A93S, clone p-Y689, Rockland), a 1:1,000 dilution of rabbit anti-STAT2 (catalog number 4594, Cell Signaling), a 1:1,000 dilution of rabbit anti-phospho-STAT3 (catalog number 9134P, clone Y705, Cell Signaling), a 1:1,000 dilution of mouse anti-STAT3 (catalog number 9139P, clone 124H6, Cell Signaling), a 1:1,000 dilution of rabbit anti-MX1 (catalog number 13750-1-AP, Proteintech), a 1:1,000 dilution of rabbit anti-MX2 (catalog number 43924S, clone E7Y8H, Cell Signaling), a 1:1,000 dilution of rabbit anti-IFI16 (catalog number 14970S, clone D8B5T, Cell Signaling), a 1:1,000 dilution of rabbit anti-APOBEC3B (catalog number 41494S, clone E9A2G, Cell Signaling), a 1:1,000 dilution of rabbit anti-ISG15 (catalog number 2758S, clone 22D2, Cell Signaling), a 1:1,000 dilution of rabbit anti-CDK14-PFTK1 (catalog number 21612-1-AP, Proteintech), a 1:1,000 dilution of rabbit anti-LARGE2/GYLTL1B (catalog number PA5-63331, Invitrogen), a 1:1,000 dilution of rabbit anti-STING (catalog number 13647S, clone D2P2F, Cell Signaling), a 1:1,000 dilution of rabbit anti-phsopho-TBK1/NAK (catalog number 5483P, clone S172, Cell Signaling), a 1:1,000 dilution of rabbit anti-cGAS (catalog number 79978, clone E5V3W, Cell Signaling), or a 1:1,000 dilution of rabbit anti-cyclin B1 (catalog number 12231T, clone D5C10, Cell Signaling). Starbright Blue 700 goat anti-rabbit (Bio-Rad, 12004161) or anti-mouse (Bio-Rad, 12004158) IgG fluorescent secondary antibodies at 1:5,000 dilutions were used for fluorescent western blotting detection using the Chemidoc MP imaging system from Bio-Rad. To verify total protein, the membranes were stained with Coomassie blue stain.

IC50 and TCID50

For gemcitabine IC50 determination, cells were seeded into 96-well plates for approximately 50% confluence in medium supplemented with 10% FBS. On the following day, cells were treated with serial dilutions of gemcitabine (Selleck, S1714) ranging from 1,000 to 0.008 μM. A WST-8 (Dojindo, CK04) cell viability assay was performed 48 h later. For VSV IC50 and TCID50 determination, cells were seeded into 96-well plates for approximately 95% confluence in medium supplemented with 10% FBS. On the following day, cells were infected with serial dilutions of VSV ranging from MOI 0.01 to MOI 0.00006. GFP-based FFU were counted at 24 h p.i. for TCID50 using a fluorescent microscope. A WST-8 cell viability assay was performed at 120 h p.i. IC50 values were calculated using GraphPad Prism 7.04. For TCID50 determination, the Reed and Muench method was used as previously described.[75]

Statistical analysis

All statistical analyses were performed using GraphPad Prism 7.04 software. Tests used are indicated in the legends of the figures.

SUPPLEMENTAL INFORMATION

Supplemental information can be found online at https://doi.org/10.1016/j.omto.2021.11.019.

ACKNOWLEDGMENTS

The authors are grateful to Eric Hastie, Jessica Miller, Christopher Castagno, and Sara Seegers for critical review of the manuscript. The authors thank the following laboratories for kindly providing reagents for this project: Jack Rose (Yale University) for VSV-ΔM51; Asit Pattnaik (University of Nebraska) for VSV-wt(GFP); Wolfgang Neubert (Max Planck Institute of Biochemistry) for SeV-GFP-Fmut virus; Pinku Mukherjee (University of North Carolina at Charlotte) for Capan-1 and MIA PaCa-2 cells; David McConky (MD Anderson Cancer Center) for CFPAC-1 and Hs766t cells; Randall Kimple

(University of North Carolina Chapel Hill) for Capan-2 and T3M4 cells; Andrei Ivanov (University of Rochester Medical School) for HPAF-II cells; Timothy Wang (Columbia University) for AsPC-1 cells; Michael Hollingsworth (University of Nebraska Medical Center) for SUIT-2 cells; and Emmanuel Zervos (Tampa General Hospital) for HPAC cells. This study was funded to V.Z.G. by grant 1R15CA238864-01 from the National Cancer Institute, National Institutes of Health (Bethesda, Maryland, USA). We thank the UNCC Center for Biomedical Engineering and Science (CBES) for summer and conference travel support for D.G.

AUTHOR CONTRIBUTIONS

Conception and design, development of methodology: D.G., C.B., M.H., and V.Z.G. Acquisition of data: D.G., C.B., and M.H. Analysis and interpretation of data: D.G., C.B., M.H., and V.Z.G. Writing, review, and revision of the manuscript: D.G., C.B., M.H., and V.Z.G. Study supervision: V.Z.G.

DECLARATION OF INTEREST

The authors declare no competing interests.

REFERENCES

1. Orloff, M. (2016). Spotlight on talimogene laherparepvec for the treatment of melanoma lesions in the skin and lymph nodes. Oncolytic Virother *5*, 91–98. https://doi.org/10.2147/OV.S99532.

2. Donina, S., Strele, I., Proboka, G., Auzins, J., Alberts, P., Jonsson, B., Venskus, D., and Muceniece, A. (2015). Adapted ECHO-7 virus Rigvir immunotherapy (oncolytic virotherapy) prolongs survival in melanoma patients after surgical excision of the tumour in a retrospective study. Melanoma Res. *25*, 421–426. https://doi.org/10.1097/CMR.0000000000000180.

3. Garber, K. (2006). China approves world's first oncolytic virus therapy for cancer treatment. J. Natl. Cancer Inst. *98*, 298–300. https://doi.org/10.1093/jnci/djj111.

4. Hastie, E., Cataldi, M., Marriott, I., and Grdzelishvili, V.Z. (2013). Understanding and altering cell tropism of vesicular stomatitis virus. Virus Res. *176*, 16–32. https://doi.org/10.1016/j.virusres.2013.06.003.

5. Finkelshtein, D., Werman, A., Novick, D., Barak, S., and Rubinstein, M. (2013). LDL receptor and its family members serve as the cellular receptors for vesicular stomatitis virus. Proc. Natl. Acad. Sci. U S A *110*, 7306–7311. https://doi.org/10.1073/pnas.1214441110.

6. Schlegel, R., Tralka, T.S., Willingham, M.C., and Pastan, I. (1983). Inhibition of vsv binding and infectivity by phosphatidylserine - is phosphatidylserine a vsv-binding site. Cell *32*, 639–646. https://doi.org/10.1016/0092-8674(83)90483-x.

7. Carneiro, F.A., Lapido-Loureiro, P.A., Cordo, S.M., Stauffer, F., Weissmuller, G., Bianconi, M.L., Juliano, M.A., Juliano, L., Bisch, P.M., and Poian, A.T.D. (2006). Probing the interaction between vesicular stomatitis virus and phosphatidylserine. Eur. Biophys. J. Biophys. *35*, 145–154. https://doi.org/10.1007/s00249-005-0012-z.

8. Schloemer, R.H., and Wagner, R.R. (1975). Cellular adsorption function of the sialoglycoprotein of vesicular stomatitis virus and its neuraminic acid. J. Virol. *15*, 882–893. https://doi.org/10.1128/JVI.15.4.882-893.1975.

9. Guibinga, G.H., Miyanohara, A., Esko, J.D., and Friedmann, T. (2002). Cell surface heparan sulfate is a receptor for attachment of envelope protein-free retrovirus-like particles and VSV-G pseudotyped MLV-derived retrovirus vectors to target cells. Mol. Ther. *5*, 538–546. https://doi.org/10.1006/mthe.2002.0578.

10. Stojdl, D.F., Lichty, B., Knowles, S., Marius, R., Atkins, H., Sonenberg, N., and Bell, J.C. (2000). Exploiting tumor-specific defects in the interferon pathway with a previously unknown oncolytic virus. Nat. Med. *6*, 821–825. https://doi.org/10.1038/77558.

11. Lichty, B.D., Power, A.T., Stojdl, D.F., and Bell, J.C. (2004). Vesicular stomatitis virus: re-inventing the bullet. Trends Mol. Med. *10*, 210–216. https://doi.org/10.1016/j.molmed.2004.03.003.

12. Zhang, K.X., Matsui, Y., Hadaschik, B.A., Lee, C., Jia, W., Bell, J.C., Fazli, L., So, A.I., and Rennie, P.S. (2010). Down-regulation of type I interferon receptor sensitizes bladder cancer cells to vesicular stomatitis virus-induced cell death. Int. J. Cancer *127*, 830–838. https://doi.org/10.1002/ijc.25088.

13. Wang, B.X., Rahbar, R., and Fish, E.N. (2011). Interferon: current status and future prospects in cancer therapy. J. Interferon Cytokine Res. *31*, 545–552. https://doi.org/10.1089/jir.2010.0158.

14. Siegel, R.L., Miller, K.D., and Jemal, A. (2020). Cancer statistics, 2020. CA Cancer J. Clin. *70*, 7–30. https://doi.org/10.3322/caac.21590.

15. Orth, M., Metzger, P., Gerum, S., Mayerle, J., Schneider, G., Belka, C., Schnurr, M., and Lauber, K. (2019). Pancreatic ductal adenocarcinoma: biological hallmarks, current status, and future perspectives of combined modality treatment approaches. Radiat. Oncol. *14*, 141. https://doi.org/10.1186/s13014-019-1345-6.

16. Zeng, S., Pottler, M., Lan, B., Grutzmann, R., Pilarsky, C., and Yang, H. (2019). Chemoresistance in pancreatic cancer. Int. J. Mol. Sci. *20*, 4504. https://doi.org/10.3390/ijms20184504.

17. Murphy, A.M., Besmer, D.M., Moerdyk-Schauwecker, M., Moestl, N., Ornelles, D.A., Mukherjee, P., and Grdzelishvili, V.Z. (2012). Vesicular stomatitis virus as an oncolytic agent against pancreatic ductal adenocarcinoma. J. Virol. *86*, 3073–3087. https://doi.org/10.1128/JVI.05640-11.

18. Moerdyk-Schauwecker, M., Shah, N.R., Murphy, A.M., Hastie, E., Mukherjee, P., and Grdzelishvili, V.Z. (2013). Resistance of pancreatic cancer cells to oncolytic vesicular stomatitis virus: role of type I interferon signaling. Virology *436*, 221–234. https://doi.org/10.1016/j.virol.2012.11.014.

19. Hastie, E., Cataldi, M., Moerdyk-Schauwecker, M.J., Felt, S.A., Steuerwald, N., and Grdzelishvili, V.Z. (2016). Novel biomarkers of resistance of pancreatic cancer cells to oncolytic vesicular stomatitis virus. Oncotarget *7*, 61601–61618. https://doi.org/10.18632/oncotarget.11202.

20. Hastie, E., Cataldi, M., Steuerwald, N., and Grdzelishvili, V.Z. (2015). An unexpected inhibition of antiviral signaling by virus-encoded tumor suppressor p53 in pancreatic cancer cells. Virology *483*, 126–140. https://doi.org/10.1016/j.virol.2015.04.017.

21. Felt, S.A., Droby, G.N., and Grdzelishvili, V.Z. (2017). Ruxolitinib and polycation combination treatment overcomes multiple mechanisms of resistance of pancreatic cancer cells to oncolytic vesicular stomatitis virus. J. Virol. *91*, e00461. https://doi.org/10.1128/JVI.00461-17.

22. Felt, S.A., Moerdyk-Schauwecker, M.J., and Grdzelishvili, V.Z. (2015). Induction of apoptosis in pancreatic cancer cells by vesicular stomatitis virus. Virology *474*, 163–173. https://doi.org/10.1016/j.virol.2014.10.026.

23. Holbrook, M.C., Goad, D.W., and Grdzelishvili, V.Z. (2021). Expanding the spectrum of pancreatic cancers responsive to vesicular stomatitis virus-based oncolytic virotherapy: challenges and solutions. Cancers *13*, 1171. https://doi.org/10.3390/cancers13051171.

24. Amrutkar, M., and Gladhaug, I.P. (2017). Pancreatic cancer chemoresistance to gemcitabine. Cancers *9*, 157. https://doi.org/10.3390/cancers9110157.

25. Weichselbaum, R.R., Ishwaran, H., Yoon, T., Nuyten, D.S., Baker, S.W., Khodarev, N., Su, A.W., Shaikh, A.Y., Roach, P., Kreike, B., et al. (2008). An interferon-related gene signature for DNA damage resistance is a predictive marker for chemotherapy and radiation for breast cancer. Proc. Natl. Acad. Sci. U S A *105*, 18490–18495. https://doi.org/10.1073/pnas.0809242105.

26. Erdal, E., Haider, S., Rehwinkel, J., Harris, A.L., and McHugh, P.J. (2017). A prosurvival DNA damage-induced cytoplasmic interferon response is mediated by end resection factors and is limited by Trex1. Genes Dev. *31*, 353–369. https://doi.org/10.1101/gad.289769.116.

27. Padariya, M., Sznarkowska, A., Kote, S., Gomez-Herranz, M., Mikac, S., Pilch, M., Alfaro, J., Fahraeus, R., Hupp, T., and Kalathiya, U. (2021). Functional interfaces, biological pathways, and regulations of interferon-related DNA damage resistance signature (IRDS) genes. Biomolecules *11*, 622. https://doi.org/10.3390/biom11050622.

28. Budhwani, M., Mazzieri, R., and Dolcetti, R. (2018). Plasticity of type I interferon-mediated responses in cancer therapy: from anti-tumor immunity to resistance. Front. Oncol. *8*, 322. https://doi.org/10.3389/fonc.2018.00322.

29. Cataldi, M., Shah, N.R., Felt, S.A., and Grdzelishvili, V.Z. (2015). Breaking resistance of pancreatic cancer cells to an attenuated vesicular stomatitis virus through a novel

activity of IKK inhibitor TPCA-1. Virology *485*, 340–354. https://doi.org/10.1016/j.virol.2015.08.003.

30. Iwamura, T., Katsuki, T., and Ide, K. (1987). Establishment and characterization of a human pancreatic-cancer cell-line (Suit-2) producing carcinoembryonic antigen and carbohydrate antigen-19-9. Jpn. J. Cancer Res. *78*, 54–62.

31. Quint, K., Tonigold, M., Di Fazio, P., Montalbano, R., Lingelbach, S., Ruckert, F., Alinger, B., Ocker, M., and Neureiter, D. (2012). Pancreatic cancer cells surviving gemcitabine treatment express markers of stem cell differentiation and epithelial-mesenchymal transition. Int. J. Oncol. *41*, 2093–2102. https://doi.org/10.3892/ijo.2012.1648.

32. Samulitis, B.K., Pond, K.W., Pond, E., Cress, A.E., Patel, H., Wisner, L., Patel, C., Dorr, R.T., and Landowski, T.H. (2015). Gemcitabine resistant pancreatic cancer cell lines acquire an invasive phenotype with collateral hypersensitivity to histone deacetylase inhibitors. Cancer Biol. Ther. *16*, 43–51. https://doi.org/10.4161/15384047.2014.986967.

33. Black, B.L., Rhodes, R.B., McKenzie, M., and Lyles, D.S. (1993). The role of vesicular stomatitis virus matrix protein in inhibition of host-directed gene expression is genetically separable from its function in virus assembly. J. Virol. *67*, 4814–4821. https://doi.org/10.1128/JVI.67.8.4814-4821.1993.

34. Stojdl, D.F., Lichty, B.D., tenOever, B.R., Paterson, J.M., Power, A.T., Knowles, S., Marius, R., Reynard, J., Poliquin, L., Atkins, H., et al. (2003). VSV strains with defects in their ability to shutdown innate immunity are potent systemic anti-cancer agents. Cancer Cell *4*, 263–275. https://doi.org/10.1016/s1535-6108(03)00241-1.

35. Hastie, E., and Grdzelishvili, V.Z. (2012). Vesicular stomatitis virus as a flexible platform for oncolytic virotherapy against cancer. J. Gen. Virol. *93*, 2529–2545. https://doi.org/10.1099/vir.0.046672-0.

36. Wollmann, G., Rogulin, V., Simon, I., Rose, J.K., and van den Pol, A.N. (2010). Some attenuated variants of vesicular stomatitis virus show enhanced oncolytic activity against human glioblastoma cells relative to normal brain cells. J. Virol. *84*, 1563–1573. https://doi.org/10.1128/JVI.02040-09.

37. Mazewski, C., Perez, R.E., Fish, E.N., and Platanias, L.C. (2020). Type I interferon (IFN)-Regulated activation of canonical and non-canonical signaling pathways. Front Immunol. *11*, 606456. https://doi.org/10.3389/fimmu.2020.606456.

38. Musella, M., Manic, G., De Maria, R., Vitale, I., and Sistigu, A. (2017). Type-I-interferons in infection and cancer: unanticipated dynamics with therapeutic implications. Oncoimmunology *6*, e1314424. https://doi.org/10.1080/2162402X.2017.1314424.

39. Chen, K., Liu, J., and Cao, X. (2017). Regulation of type I interferon signaling in immunity and inflammation: a comprehensive review. J. Autoimmun. *83*, 1–11. https://doi.org/10.1016/j.jaut.2017.03.008.

40. Arimoto, K.I., Miyauchi, S., Stoner, S.A., Fan, J.B., and Zhang, D.E. (2018). Negative regulation of type I IFN signaling. J. Leukoc. Biol. *103*, 1099–1116. https://doi.org/10.1002/JLB.2MIR0817-342R.

41. Zitvogel, L., Galluzzi, L., Kepp, O., Smyth, M.J., and Kroemer, G. (2015). Type I interferons in anticancer immunity. Nat. Rev. Immunol. *15*, 405–414. https://doi.org/10.1038/nri3845.

42. Snell, L.M., McGaha, T.L., and Brooks, D.G. (2017). Type I interferon in chronic virus infection and cancer. Trends Immunol. *38*, 542–557. https://doi.org/10.1016/j.it.2017.05.005.

43. Duarte, C.W., Willey, C.D., Zhi, D., Cui, X., Harris, J.J., Vaughan, L.K., Mehta, T., McCubrey, R.O., Khodarev, N.N., Weichselbaum, R.R., and Gillespie, G.Y. (2012). Expression signature of IFN/STAT1 signaling genes predicts poor survival outcome in glioblastoma multiforme in a subtype-specific manner. PLoS One *7*, e29653. https://doi.org/10.1371/journal.pone.0029653.

44. Rickardson, L., Fryknas, M., Dhar, S., Lovborg, H., Gullbo, J., Rydaker, M., Nygren, P., Gustafsson, M.G., Larsson, R., and Isaksson, A. (2005). Identification of molecular mechanisms for cellular drug resistance by combining drug activity and gene expression profiles. Br. J. Cancer *93*, 483–492. https://doi.org/10.1038/sj.bjc.6602699.

45. Prieto-Vila, M., Takahashi, R.U., Usuba, W., Kohama, I., and Ochiya, T. (2017). Drug resistance driven by cancer stem cells and their Niche. Int. J. Mol. Sci. *18*, 2574. https://doi.org/10.3390/ijms18122574.

46. Cai, Z., Cao, Y., Luo, Y., Hu, H., and Ling, H. (2018). Signalling mechanism(s) of epithelial-mesenchymal transition and cancer stem cells in tumour therapeutic resistance. Clin. Chim. Acta *483*, 156–163. https://doi.org/10.1016/j.cca.2018.04.033.

47. Boelens, M.C., Wu, T.J., Nabet, B.Y., Xu, B., Qiu, Y., Yoon, T., Azzam, D.J., Twyman-Saint Victor, C., Wiemann, B.Z., Ishwaran, H., et al. (2014). Exosome transfer from stromal to breast cancer cells regulates therapy resistance pathways. Cell *159*, 499–513. https://doi.org/10.1016/j.cell.2014.09.051.

48. Brass, A.L., Huang, I.C., Benita, Y., John, S.P., Krishnan, M.N., Feeley, E.M., Ryan, B.J., Weyer, J.L., van der Weyden, L., Fikrig, E., et al. (2009). The IFITM proteins mediate cellular resistance to influenza A H1N1 virus, West Nile virus, and dengue virus. Cell *139*, 1243–1254. https://doi.org/10.1016/j.cell.2009.12.017.

49. Andreu, P., Colnot, S., Godard, C., Laurent-Puig, P., Lamarque, D., Kahn, A., Perret, C., and Romagnolo, B. (2006). Identification of the IFITM family as a new molecular marker in human colorectal tumors. Cancer Res. *66*, 1949–1955. https://doi.org/10.1158/0008-5472.CAN-05-2731.

50. Kita, K., Sugaya, S., Zhai, L., Wu, Y.P., Wano, C., Chigira, S., Nomura, J., Takahashi, S., Ichinose, M., and Suzuki, N. (2003). Involvement of LEU13 in interferon-induced refractoriness of human RSa cells to cell killing by X rays. Radiat. Res. *160*, 302–308. https://doi.org/10.1667/rr3039.

51. Gaston, J., Cheradame, L., Yvonnet, V., Deas, O., Poupon, M.F., Judde, J.G., Cairo, S., and Goffin, V. (2016). Intracellular STING inactivation sensitizes breast cancer cells to genotoxic agents. Oncotarget *7*, 77205–77224. https://doi.org/10.18632/oncotarget.12858.

52. Cheon, H., and Stark, G.R. (2009). Unphosphorylated STAT1 prolongs the expression of interferon-induced immune regulatory genes. Proc. Natl. Acad. Sci. U S A *106*, 9373–9378. https://doi.org/10.1073/pnas.0903487106.

53. Nan, Y., Wu, C., and Zhang, Y.J. (2018). Interferon independent non-canonical STAT activation and virus induced inflammation. Viruses *10*, 196. https://doi.org/10.3390/v10040196.

54. Li, Z., Chen, C., Chen, L., Hu, D., Yang, X., Zhuo, W., Chen, Y., Yang, J., Zhou, Y., Mao, M., et al. (2021). STAT5a confers doxorubicin resistance to breast cancer by regulating ABCB1. Front Oncol. *11*, 697950. https://doi.org/10.3389/fonc.2021.697950.

55. Mendoza-Rodriguez, M.G., Sanchez-Barrera, C.A., Callejas, B.E., Garcia-Castillo, V., Beristain-Terrazas, D.L., Delgado-Buenrostro, N.L., Chirino, Y.I., Leon-Cabrera, S.A., Rodriguez-Sosa, M., Gutierrez-Cirlos, E.B., et al. (2020). Use of STAT6 phosphorylation inhibitor and trimethylglycine as new adjuvant therapies for 5-fluorouracil in colitis-associated tumorigenesis. Int. J. Mol. Sci. *21*, 2130. https://doi.org/10.3390/ijms21062130.

56. Leon-Cabrera, S.A., Molina-Guzman, E., Delgado-Ramirez, Y.G., Vazquez-Sandoval, A., Ledesma-Soto, Y., Perez-Plasencia, C.G., Chirino, Y.I., Delgado-Buenrostro, N.L., Rodriguez-Sosa, M., Vaca-Paniagua, F., et al. (2017). Lack of STAT6 attenuates inflammation and drives protection against early steps of colitis-associated colon cancer. Cancer Immunol. Res. *5*, 385–396. https://doi.org/10.1158/2326-6066.CIR-16-0168.

57. Natoli, A., Lupertz, R., Merz, C., Muller, W.W., Kohler, R., Krammer, P.H., and Li-Weber, M. (2013). Targeting the IL-4/IL-13 signaling pathway sensitizes Hodgkin lymphoma cells to chemotherapeutic drugs. Int. J. Cancer *133*, 1945–1954. https://doi.org/10.1002/ijc.28189.

58. Fish, E.N., Uddin, S., Korkmaz, M., Majchrzak, B., Druker, B.J., and Platanias, L.C. (1999). Activation of a CrkL-stat5 signaling complex by type I interferons. J. Biol. Chem. *274*, 571–573. https://doi.org/10.1074/jbc.274.2.571.

59. Gupta, S., Jiang, M., and Pernis, A.B. (1999). IFN-alpha activates Stat6 and leads to the formation of Stat2:Stat6 complexes in B cells. J. Immunol. *163*, 3834–3841.

60. Ashley, C.L., Abendroth, A., McSharry, B.P., and Slobedman, B. (2019). Interferon-independent upregulation of interferon-stimulated genes during human cytomegalovirus infection is dependent on IRF3 expression. Viruses *11*, 246. https://doi.org/10.3390/v11030246.

61. Grandvaux, N., Servant, M.J., tenOever, B., Sen, G.C., Balachandran, S., Barber, G.N., Lin, R., and Hiscott, J. (2002). Transcriptional profiling of interferon regulatory factor 3 target genes: direct involvement in the regulation of interferon-stimulated genes. J. Virol. *76*, 5532–5539. https://doi.org/10.1128/jvi.76.11.5532-5539.2002.

62. Khodarev, N.N., Minn, A.J., Efimova, E.V., Darga, T.E., Labay, E., Beckett, M., Mauceri, H.J., Roizman, B., and Weichselbaum, R.R. (2007). Signal transducer and activator of transcription 1 regulates both cytotoxic and prosurvival functions in

tumor cells. Cancer Res. *67*, 9214–9220. https://doi.org/10.1158/0008-5472.CAN-07-1019.

63. Das, S.C., Nayak, D., Zhou, Y., and Pattnaik, A.K. (2006). Visualization of intracellular transport of vesicular stomatitis virus nucleocapsids in living cells. J. Virol. *80*, 6368–6377. https://doi.org/10.1128/JVI.00211-06.

64. Wiegand, M.A., Bossow, S., Schlecht, S., and Neubert, W.J. (2007). De novo synthesis of N and P proteins as a key step in Sendai virus gene expression. J. Virol. *81*, 13835–13844. https://doi.org/10.1128/JVI.00914-07.

65. Metzgar, R.S., Gaillard, M.T., Levine, S.J., Tuck, F.L., Bossen, E.H., and Borowitz, M.J. (1982). Antigens of human pancreatic adenocarcinoma cells defined by murine monoclonal antibodies. Cancer Res. *42*, 601–608.

66. Chen, W.H., Horoszewicz, J.S., Leong, S.S., Shimano, T., Penetrante, R., Sanders, W.H., Berjian, R., Douglass, H.O., Martin, E.W., and Chu, T.M. (1982). Human pancreatic adenocarcinoma: in vitro and in vivo morphology of a new tumor line established from ascites. In Vitro *18*, 24–34. https://doi.org/10.1007/BF02796382.

67. Kyriazis, A.P., Kyriazis, A.A., Scarpelli, D.G., Fogh, J., Rao, M.S., and Lepera, R. (1982). Human pancreatic adenocarcinoma line Capan-1 in tissue culture and the nude mouse: morphologic, biologic, and biochemical characteristics. Am. J. Pathol. *106*, 250–260.

68. Kyriazis, A.A., Kyriazis, A.P., Sternberg, C.N., Sloane, N.H., and Loveless, J.D. (1986). Morphological, biological, biochemical, and karyotypic characteristics of human pancreatic ductal adenocarcinoma Capan-2 in tissue culture and the nude mouse. Cancer Res. *46*, 5810–5815.

69. Schoumacher, R.A., Ram, J., Iannuzzi, M.C., Bradbury, N.A., Wallace, R.W., Hon, C.T., Kelly, D.R., Schmid, S.M., Gelder, F.B., Rado, T.A., et al. (1990). A cystic fibrosis pancreatic adenocarcinoma cell line. Proc. Natl. Acad. Sci. U S A *87*, 4012–4016. https://doi.org/10.1073/pnas.87.10.4012.

70. Yunis, A.A., Arimura, G.K., and Russin, D.J. (1977). Human pancreatic carcinoma (MIA PaCa-2) in continuous culture: sensitivity to asparaginase. Int. J. Cancer *19*, 128–135. https://doi.org/10.1002/ijc.2910190118.

71. Gower, W.R., Jr., Risch, R.M., Godellas, C.V., and Fabri, P.J. (1994). HPAC, a new human glucocorticoid-sensitive pancreatic ductal adenocarcinoma cell line. In Vitro Cell Dev. Biol. Anim. *30A*, 151–161. https://doi.org/10.1007/BF02631438.

72. Okabe, T., Yamaguchi, N., and Ohsawa, N. (1983). Establishment and characterization of a carcinoembryonic antigen (CEA)-producing cell line from a human carcinoma of the exocrine pancreas. Cancer *51*, 662–668. https://doi.org/10.1002/1097-0142(19830215)51:4<662::aid-cncr2820510419>3.0.co;2-x.

73. Owens, R.B., Smith, H.S., Nelson-Rees, W.A., and Springer, E.L. (1976). Epithelial cell cultures from normal and cancerous human tissues. J. Natl. Cancer Inst. *56*, 843–849. https://doi.org/10.1093/jnci/56.4.843.

74. Bressy, C., Droby, G.N., Maldonado, B.D., Steuerwald, N., and Grdzelishvili, V.Z. (2019). Cell cycle arrest in G(2)/M phase enhances replication of interferon-sensitive cytoplasmic RNA viruses via inhibition of antiviral gene expression. J. Virol. *93*, e01885. https://doi.org/10.1128/JVI.01885-18.

75. Ramakrishnan, M.A. (2016). Determination of 50% endpoint titer using a simple formula. World J. Virol. *5*, 85–86. https://doi.org/10.5501/wjv.v5.i2.85.